PHYSICAL REVIEW A VOLUME 16, NUMBER 6 DECEMBER 1977

Collision-induced absorption in atomic electronic transitions

Alan Gallagher
Joint Institute for Laboratory Astrophysics, National Bureau of Standards and University of Colorado, Boulder, Colorado 80309

T. Holstein
Physics Department, University of California at Los Angeles, Los Angeles, California 90024
(Received 16 June 1977)

The collision-induced absorption and emission coefficients for electric-dipole forbidden atomic transitions are calculated for weak radiation fields. The approximations used are valid for $\hbar\omega$ near $\hbar\omega_0$, the atomic energy differences. The example case of S-D transitions induced by a spherically symmetric perturber (e.g., a noble-gas atom) is treated in detail and compared to measurements. The case of "radiative collisions," in which both colliding atoms change their state, is included in the theory and is also compared to experiment.

I. INTRODUCTION

This paper calculates electric-dipole absorption (emission) coefficients for electronic transitions that only absorb (emit) radiation during a collision between two atoms. We treat the weak-field limit, with absorption proportional to the radiation intensity, and restrict the calculation to frequencies near ω_0, where $\hbar\omega_0$ is the energy spacing of the separated atomic states. We interpret this process in terms of radiative transitions, generally free-free, between electronic states α and α' of a diatomic molecule. The *dipole-forbidden* character of the transition for the *separated atoms* is then transformed to an electric-dipole transition moment of the molecule $\mu(R)_{\alpha\to\alpha'}$ which becomes zero as the internuclear separation $R\to\infty$. Two classes of forbidden transitions of the separated atoms are treated equivalently in this model, yielding the same basic line-core shapes. The first class in which only one atom changes state is

$$A(n)+B(n_1)\to A(n')+B(n_1)\pm\hbar\omega, \tag{1}$$

where $A(n)\to A(n')$ is not a dipole-allowed transition; n is an abbreviation for the quantum number n, L, S, J, M_J; and we neglect nuclear spin. This process has been observed in absorption and emission[1-6] and has been qualitatively explained for a long time,[1] but three recently observed cases stimulate interest in a general, quantitative theory. One of these is the laser transition[3]

$$\mathrm{O}(^1D)+\mathrm{Xe}(^1S_0)\to\mathrm{O}(^1S)+\mathrm{Xe}(^1S_0)+\hbar\omega, \tag{1a}$$

for which a very thorough but specific theory has been developed.[4] The second[5] is the first quantitative measurements of the process in Eq. (1). An example case from Ref. 5 is

$$\mathrm{Cs}(6\,^2S)+\mathrm{Ar}(^1S_0)+\hbar\omega\to\mathrm{Cs}(5\,^2D)+\mathrm{Ar}(^1S_0). \tag{1b}$$

The third is a more recent quantitative measurement for the process in Eq. (1b) with $\mathrm{Ar}(^1S_0)$ replaced by $\mathrm{Cs}(6\,^2S_{1/2})$.[6]

The second class in which both atoms change state was called "radiative collisions" in the original articles,[7] i.e.,

$$A(n)+B(n_1)\to A(n')+B(n_1')\pm\hbar\omega. \tag{2}$$

The basic description of this process is given in Ref. 7, and it has also received considerable attention recently.[8-11] Measurements have been reported for[8,9]

$$\mathrm{Sr}(5\,^1P)+\mathrm{Ca}(4\,^1S)+\hbar\omega\to\mathrm{Sr}(5\,^1S)+\mathrm{Ca}(5\,^1D\text{ or }6\,^1S). \tag{2a}$$

Equation (2a) is clearly representative of a wide range of mixed atom-pair absorptions, such as the reverse of the reaction in Eq. (2b). To observe the process of Eq. (2) in emission is difficult due to competing collision processes, but an example which should be observable at visible wavelengths is

$$\mathrm{Ca}(4\,^1P_1)+\mathrm{Tl}(6\,^2P_{1/2})\to\mathrm{Ca}(4\,^1S_0)+\mathrm{Tl}(6\,^2P_{3/2})+\hbar\omega, \tag{2b}$$

where any group IIA and IIIA elements might be substituted for Ca and Tl.

To calculate the line shapes and intensities for the processes of Eqs. (1) and (2), which are dipole forbidden at large internuclear separation, we have utilized the traditional method, based on the Born-Oppenheimer approximation and Franck-Condon principle, that is used to calculate collisionally-broadened line shapes of dipole-allowed atomic transitions.[12] For either the present dipole-forbidden or the normal dipole-allowed cases the far wings, at $|\omega-\omega_0|\gg 1/\tau_c$, where τ_c is a characteristic time of collision, are described by the quasistatic theory, which is equivalent to using the classical Franck-Condon principle.[12] For both

the dipole-allowed and forbidden cases the line wing intensities are proportional to $[A(n)][B(n_1)]$, where [ ] refers to species density. For the dipole-allowed case, the line core at $|\omega - \omega_0| \leq 1/\tau_c$ is Lorentzian shaped with an area proportional to $[A(n)]$. In the present dipole-forbidden case the line core intensity is proportional to $[A(n)][B(n_1)]$ and its non-Lorentzian shape is the subject of the present work.

Our molecular state model is equivalent to the previous qualitative description[1] of process (1b) as due to excited P-state components collisionally mixed into the ground S state, allowing an electric-dipole transition to an excited D state. The existing theories of "radiative collisions" use a different language to describe process (2), but also consider the same interactions as those evaluated here. Thus we arrive at equations for line shape and cross sections that are similar to those in Refs. 7–9; the primary differences are due to a more detailed treatment of M dependence and molecular axis rotation here. In addition, the equations are numerically integrated.

We believe that for low light intensities or spontaneous emission there are distinct advantages to the molecular-transition language and model for these processes. This model treats the line core and wings of class (1) and (2) processes in a consistent fashion, points out the equivalence of these two classes of processes and their line shapes, and fits this description into the familiar, highly developed, and very universal theories of line broadening and molecular radiation. In fact, the class (1) process has already been calculated for the case of electron perturbers[13] by this "traditional" method, resulting in the same characteristic type of line-shape equations that are obtained here for both class (1) and (2) cases. Within the framework and approximations of the present theory, a great variety of specific type (1) and (2) cases have either of two line-core shapes, one due to the long-range dipole-dipole interaction and one for the dipole-quadrupole interaction. We have numerically evaluated the line-shape triple integrals in order to provide tabulations of these two very general theoretical line shapes and to allow quantitative comparisons with experiments.

II. THEORY

A. Approximations

The several approximations used are (i) the Born-Oppenheimer approximation, with neglect of nonadiabatic terms between nondegenerate states; (ii) the long-range multipole expansion of the electrostatic interaction between atoms A and B is used as a perturbation to obtain the molecular adiabatic states and their potential energies, and only the leading terms are included; (iii) straight-line-path collision orbits; (iv) no nonadiabatic mixing of molecular M levels (this is the most important neglected nonadiabatic term at large R, as these states are nearly degenerate); (v) no change in nuclear angular momentum in the radiative transition, as is implicit in the straight-line path assumption (this is equivalent to neglecting the differences between P, Q, and R branches); (vi) no change in L-S coupling scheme (Hund's case), which is consistent with assumption (iv); and (vii) weak radiation field, no radiation-induced level shifts or saturation.

The first approximation is quite valid in this treatment of thermal vapors and transitions between electronic states that are isolated at large R. The second and third assumptions are appropriate only for calculations of the line core and near wings, as these are primarily due to weak large-R interaction energies. As $|\omega - \omega_0|$ increases, the dominant R region responsible for each $\omega \to \omega + d\omega$ portion of the spectrum generally decreases. We use a large R approximation for the molecular adiabatic potentials and transition moments, which breaks down as R decreases. Thus our results are only valid within a limited $|\omega - \omega_0|$ region. This range of validity depends on the specific case; criteria and examples will be discussed below. Assumption vi also breaks down when R decreases to a value where the interaction energies are nonnegligible compared to fine-structure splittings.

Assumption ii also limits the applicability of the present results to transitions where n and n' (and n_1 and n_1') have the same spin. Approximations iv and v are traditional in most line-shape calculations for allowed lines due to the complexity involved in removing them and the supposition that they have a minor effect.[12] They have been included in some calculations (e.g., Ref. 14) but it is not easy to generalize from these. The effect of M mixing on the broadening of an allowed transition with a long-range Van der Waals interaction has been shown to be minor.[15] It is unlikely that the inaccuracies arising from assumptions iv and v exceed those from assumption ii, which can only be improved by using more accurate molecular states and potentials, as in Ref. 4. The present theory, although less accurate, is intended to have general applicability.

The evaluation of a molecular free-free transition probability as occurring between electronic states which result from an orbit $\vec{R}(\vec{b}, \vec{v}, t)$ can be shown to be equivalent to evaluating Franck-Condon factors using WKB wave functions for the nuclear motion ($\vec{b}$ is the impact parameter and $\vec{v}$ the initial interatomic velocity). Thus it is valid when

$K^{-2}\,dK/dR \ll 1$, equivalent to $(\lambda\!\!\!^{-}_N\, dV/dR)/k_BT \ll 1$, where $\hbar K$ is the internuclear momentum, $K^{-1} = \lambda\!\!\!^{-}_N$, k_BT is the characteristic collision energy, and $V(R)$ is the adiabatic molecular potential. For $|\Delta V| \propto R^{-6}$, where $\Delta V = V(R) - V(\infty)$, this reduces to $(\lambda\!\!\!^{-}_N/R)(|\Delta V|/k_BT) \ll 1$, which for thermal collisions between heavy atoms at typical distances of 5 Å becomes $|\Delta V(\mathrm{cm}^{-1})| \ll 10^4$. In the present work, $|\Delta V(\mathrm{cm}^{-1})| \ll 10^2$, so this condition is well satisfied.

Transitions from weakly bound states also contribute to the measured intensities. Their contribution to the continuum intensity distribution is insignificant for $|\Delta V|/k_BT \ll 1$, which characterizes the line core of the present calculations. Thus they are neglected in the line-core calculation. These contributions as well as curvilinear trajectories are significant in the far wings, and they are included in the $\exp(-\Delta V/kT)$ factor of the quasistatic theory that is used here for the far-wing intensities.[16,17]

B. The model

In our model the large R adiabatic molecular states are expanded as a sum of atomic basis states $|A(n)B(n_1)\rangle$, and we take

$$V_{\text{electrostatic}} = V_A + V_B + V'(R),$$

with V_i the electrostatic potential for isolated atom i, and

$$V'(R) = V_{dd} + V_{dq} + V_{qd} + \cdots.$$

$$V_{dd} = \{\vec{r}_A \cdot \vec{r}_B - 3(\vec{r}_A \cdot \hat{R})(\vec{r}_B \cdot \vec{R})\}R^{-3}$$

is the familiar dipole-dipole interaction potential with $\vec{r}_A = \Sigma r_j$ over electron coordinates of atom A, $V_{qd} + V_{dq} \propto R^{-4}$ are the dipole-quadrupole interaction potentials, etc.[18] We use perturbation theory, with perturbation $V'(R)$, to obtain each adiabatic state as a sum of $|A(n)B(n_1)\rangle$ basis states with R-dependent coefficients from first order and electronic potential energies from second order. Straight-line collision orbits are used to obtain $R(t)$ and thereby the time dependence of the coefficients and electronic state energies. A weak electric-dipole radiation field perturbation $[V_r(t) = (\vec{E}_0 \cos\omega t)\cdot e\vec{r}]$ is then introduced as a perturbation between two of these time-dependent electronic molecular states and the net transition probability for a single collision is calculated ($\vec{r}$ represents a sum over all electrons $\vec{r}_i$). The collisional average over $\vec{b}, \vec{v}$ of the absorption (emission) then yields the absorption (emission) coefficient.

The dominant molecular electronic transition moment between adiabatic states occurs between the initial product basis states and those that are mixed in by $V'(R)$, so that the transition can be considered as arising from the successive application, in either order, of $V'[R(t)]$ and $V_r(t)$ perturbations. The $V_r(t)$ perturbation is a one-electron operator, so it only changes the electronic state of one atom. For the example in Eq. (1b) the transition can be shown diagrammatically as

$$\mathrm{Cs}(6\,^2S_{1/2})\mathrm{Xe}(5\,^1S_0) \xrightarrow{V_{qd}} \sum_{k_1} \mathrm{Cs}(5\,^2D_J)\mathrm{Xe}(k_1\,^1P_1) \xrightarrow{V_r} \mathrm{Cs}(5\,^2D_J)\mathrm{Xe}(5\,^1S_0), \qquad (1b')$$
$$\mathrm{Cs}(6\,^2S_{1/2})\mathrm{Xe}(5\,^1S_0) \xrightarrow{V_r} \sum_{k_1'} \mathrm{Cs}(6\,^2S_{1/2})\mathrm{Xe}(k_1'\,^1P_1) \xrightarrow{V_{qd}} \mathrm{Cs}(5\,^2D_J)\mathrm{Xe}(5\,^1S_0),$$

where both channels add coherently; and for the example in (2a) as

$$\mathrm{Sr}(5\,^1P_1)\mathrm{Ca}(4\,^1S_0) \xrightarrow{V_{dd}} \sum_{k_1} \mathrm{Sr}(5\,^1S_0)\mathrm{Ca}(k_1\,^1P_1) \xrightarrow{V_r} \mathrm{Sr}(5\,^1S_0)\mathrm{Ca}(5\,^1D_2 \text{ or } 6\,^1S_0). \qquad (2a')$$
$$\mathrm{Sr}(5\,^1P_1)\mathrm{Ca}(4\,^1S_0) \xrightarrow{V_r} \sum_{k_1'} \mathrm{Sr}(5\,^1P_1)\mathrm{Ca}(k_1'\,^1P_1) \xrightarrow{V_{dd}} \mathrm{Sr}(5\,^1S_0)\mathrm{Ca}(5\,^1D_2 \text{ or } 6\,^1S_0).$$

This successive application of collisional and radiative perturbations is essentially the same picture involved in Ref. 1 to explain collisionally induced $S \rightarrow D$ absorption. It has also been used to explain the "radiative collisions," for the case of a weak V_r as well as the high-power case where V_r cannot be treated as a perturbation.[7-9] Here we identify these collisionally mixed-in atomic states as parts of the initial and final molecular adiabatic states. In the language of line-broadening theory they could be identified with the upper-state and lower-state interactions.

The molecular-state pictures for these two example cases are shown in Figs. 1 and 2. The en-

ergies of these states are generally attractive and proportional C_6R^{-6} at large R, with increasing C_6 coefficient for decreasing atomic binding. The $\mathrm{Ca}(4\,^1P_M)\,\mathrm{Sr}(5\,^1S_0)$ state in Fig. 2 is an exception due to its proximity to $\mathrm{Ca}(4\,^1S_0)\,\mathrm{Sr}(5\,^1P_M)$. This pair of product states are mixed by the $V_{dd}(\propto R^{-3})$ interaction and their energy levels are repelled $\propto R^{-6}$ (from second-order perturbation theory). In addition to the initial and final states of the optical transitions, the figures include some of the molecular states associated with atomic product states that contribute to the transition moment, i.e., those indicated in (1b′) and (2a′). Other molecular states are indicated as unlabeled lines at the separated atom limits, as these will normally influence the transition less directly.

The present theory is closely related to the traditional theory of collisionally broadened dipole-allowed atomic transitions. For the idealized case of two isolated atomic states, each of which forms a single molecular state $V_1(R)$ or $V_2(R)$ with $V_2(\infty) - V_1(\infty) = \hbar\omega_0$, the intensity $I(\omega)$ for the dipole-allowed case results from[19]

$$I(\omega) \propto \frac{1}{2T}\left| \int_{-T}^{T} dt\, \mu_{12} \exp\left(i\omega t - i\hbar^{-1} \times \int_{-T}^{t} dt'\{V_2[R(t')] - V_1[R(t')]\}\right)\right|^2_{\mathrm{av}}, \quad (3a')$$

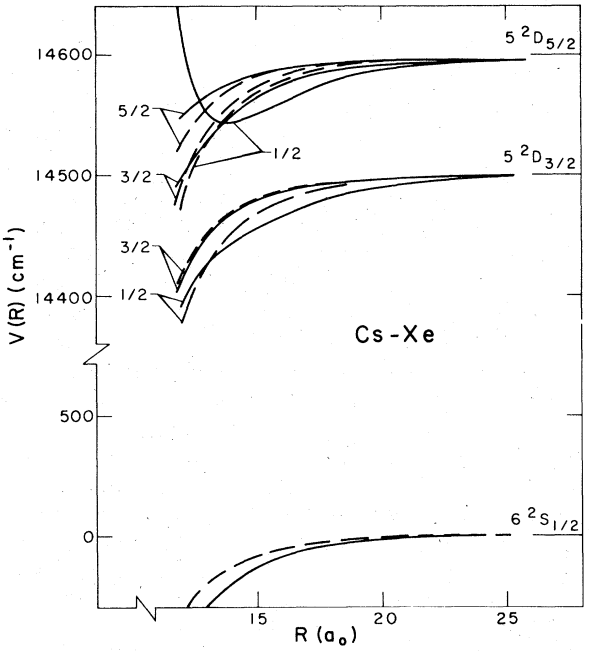

FIG. 1. Cs-Xe adiabatic potentials responsible for the Cs $6\,^2S_{1/2} \rightarrow 5\,^2D_J$ absorption coefficients. The C_6R^{-6} approximations used in the long-range theory (dashed lines) is compared to the potentials of Pascale and Vandeplanque (Ref. 22) (solid lines).

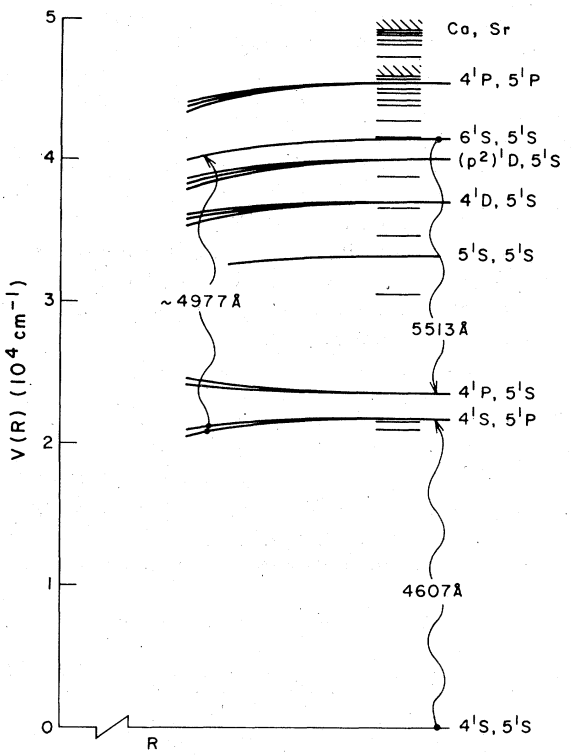

FIG. 2. Ca-Sr adiabatic potentials responsible for the $\mathrm{CaSr}^* \rightarrow \mathrm{Ca}^*\mathrm{Sr}$ ($\lambda \sim 4977$ Å) absorption coefficient, or "radiative collision." In the experiment the 5513-Å fluorescence is detected and the $\mathrm{Sr}(5\,^1P)$ is optically pumped ~ 50 cm^{-1} on the wing of the 4607-Å resonance line to avoid a background signal due to two-photon absorption by Ca.

where the average is over b and v, and μ_{12} is the electric-dipole moment, which is assumed independent of R. Here T must formally be longer than the time between collisions since the atom radiates between collisions. The impact approximation[12] yields

$$I(\omega) \propto (\tfrac{1}{2}\Gamma/\pi)/[(\tfrac{1}{2}\Gamma)^2 + (\omega - \omega_0 - \Delta)^2],$$

where the shift Δ and width Γ are given in terms of an integral through single collisions. This is valid for the central portion of the line, such that $|\omega - \omega_0| < \tau_c^{-1}$, where τ_c is the characteristic time of collision. The "static" far wing, where $|\omega - \omega_0| \gg 1/\tau_c$ also comes from the collisional portions of the above integral, with the dominant contribution from the "stationary-phase" times when the exponent traverses zero. In the dipole-forbidden case, the two-level approximation leads to a very similar expression, i.e.,

$$I(\omega) \propto \left| \int_{-\infty}^{\infty} dt\, \mu_{12}[R(t)] \exp\left(i\omega t - i\hbar^{-1} \times \int_{-\infty}^{t} dt'\{V_2[R(t')] - V_1(R(t'))\}\right)\right|^2_{\mathrm{av}}. \quad (3b')$$

Here $\mu_{12}(R)$ is the (collisionally induced) electric-dipole moment between molecular states 1 and 2. Since the atom does not radiate between collisions, the time integral can be immediately restricted to the time of one collision ($-\infty$ to ∞) for a single $\vec{b},\vec{v}$ collision. Just as for the allowed case, the stationary phase times t_s, when $\hbar\omega = V_2(t_s) - V_1(t_s)$, dominate the integral in the far wings ($|\omega - \omega_0| > 1/\tau_c$). The following theory keeps track of the molecular axis rotation and M dependences for degenerate atomic levels, but is basically represented by this simple expression.

C. General theory

We will label the adiabatic molecular states with quantum numbers αMM_1, and atomic states, as previously, with quantum numbers $nM = n, L, S, J, M$, sometimes for convenience with $\mathfrak{M}$ used in place of M. The molecular state αMM_1 is that which connects adiabatically with the separated atomic states $A(n, L, S, J, M)$ and $B(n_1, L_1, S_1, J_1, M_1)$, with α representing the $n, L, S, J, n_1, L_1, S_1, J_1$ quantum numbers. Note that, as explained in the approximation section, we do not include the mixing of these various MM_1 states by the rotation of the molecular axis. Thus we are effectively in the Hund's case (a) coupling scheme. The absorption or emission of Eqs. (1) and (2) corresponds to the $\alpha \to \alpha'$ transition and has contributions from the $(2J+1)(2J_1+1)(2J'+1)(2J_1'+1)$ different $\alpha MM_1 \to \alpha' M' M_1'$ combinations of adiabatic states. As noted above, these calculations only apply to transitions between states of atom A (and B) with the same spin, since otherwise the transition moment induced by the electrostatic perturbation $V'(R)$ is zero. The adiabatic electronic state $|\alpha MM_1(R)\rangle$ and its electronic energy $V_{\alpha MM_1}(R)$ are then given, to first order by

$$|\alpha MM_1(\vec{R})\rangle = |A(nM)B(n_1M_1)\rangle + \sum_{\substack{kk_1 \\ \mathfrak{M}\mathfrak{M}_1}} \left(\frac{\langle A(k\mathfrak{M})B(k_1\mathfrak{M}_1)|V'(\vec{R})|A(nM)B(n_1M_1)\rangle}{E_n + E_{n_1} - E_k - E_{k_1}} \right) |A(k\mathfrak{M})B(k_1\mathfrak{M}_1)\rangle, \tag{3a}$$

$$V_{\alpha MM_1}(\vec{R}) = E_n + E_{n_1} + \sum_{\substack{kk_1 \\ \mathfrak{M}\mathfrak{M}_1}} \frac{|\langle A(k\mathfrak{M})B(k_1\mathfrak{M}_1)|V'(\vec{R})|A(nM)B(n_1M_1)\rangle|^2}{E_n + E_{n_1} - E_k - E_{k_1}}. \tag{3b}$$

For convenience we will delete the vectors on $\vec{R}$, $\vec{b}$, and $\vec{v}$, as these are only relevant to the molecular-axis rotation section. In the absence of a radiation field, the time-dependent electronic-state wave function $|\alpha MM_1(t)\rangle$, subject to the collision orbit $R(b,v,t)$, can be calculated by time-dependent perturbation theory, using time-dependent basis states given by Eq. (3a) with $\vec{R} = R(t)$. When the nonadiabatic mixing is neglected, as assumed here, this yields

$$|\alpha MM_1(t)\rangle = |\alpha MM_1[R(b,v,t)]\rangle \exp i \int_{-\infty}^{t} dt' \hbar^{-1} \times V_{\alpha MM_1}[R(b,v,t')], \tag{3c}$$

where $t=0$ is defined to be at the time of closest approach.

The probability $P(b,v,\omega)$ that an $\alpha \to \alpha'$ transition occurs during a single collision due to the presence of the radiation-field perturbation $V_r(t) = \vec{E}_0 \cdot e\vec{r}\cos\omega t$ is

$$P(b,v,\omega) = \sum_{\substack{MM' \\ M_1M_1'}} \frac{1}{g_\alpha} \left| \int_{-\infty}^{\infty} dt \langle \alpha MM_1'(t) | \frac{V_r(t)}{\hbar} | \alpha' M' M_1'(t) \rangle \right|^2. \tag{4}$$

Here $g_\alpha = (2J+1)(2J_1+1)$, and we have averaged over initial and summed over final M values since the present experimental observations, in which polarization information is neglected, correspond to transitions from an initial statistical distribution of M levels to all final M levels. It can be shown that Eq. (4) also results from taking the Franck-Condon factor between stationary-state WKB nuclear wave functions of energy separation $\hbar\omega$, changing the integration variable R to t using $dt = dR/v_R(b,v)$, where $v_R(b,v) = \hbar k(b,v)/\mu$, and neglecting the difference between the R component of velocity in the initial and final-state potentials (e.g., see Ref. 17). This corresponds to the present classical-orbit approximation.

The transition rate per unit volume $T(\omega)$ is given by

$$T(\omega) = [A(n)][B(n_1)] \int_0^{\infty} 2\pi b\, db \int_0^{\infty} \rho(v) v\, dv\, P(b,v,\omega), \tag{5a}$$

where $\rho(v)$ is the normalized thermal interatomic velocity distribution, with μ the reduced mass:

$$\rho(v) = (4/\sqrt{\pi})(\mu/2kT)^{3/2} v^2 \exp(-\mu v^2/2kT) . \quad (5b)$$

The absorbed power per unit volume is $\hbar\omega T(\omega)$, the radiation field intensity is $I = E_0^2 c/8\pi$, and the absorption coefficient $k_\nu(\nu = \omega/2\pi = c/\lambda = ck)$ is given by their ratio:

$$k_\nu = 8\pi\hbar\omega T(\omega)/E_0^2 c . \quad (6)$$

The spontaneous emission I_ν and stimulated emission cross sections G_ν are given in terms of k_ν by thermodynamic relations equivalent to the Einstein A/B relations, i.e.,

$$\frac{G_\nu}{[A(n^*)][B(n_1^*)]} = \frac{k_\nu\, e^{-\hbar(\nu-\nu_0)/k_B T}}{[A(n)][B(n_1)]}$$

and $I_\nu = 8\pi G_\nu/\lambda^2$.

The process under consideration is effectively a three-body collision process, but one can define a collision cross section $Q(\omega, I)$ for the transition in the presence of a given radiation intensity I, as has been done in descriptions of "radiative collisions":

$$Q(\omega, I) = \frac{T(\omega, I)}{[A(i)][B(i_1)]\langle v_{AB}\rangle} , \quad (7)$$

where $v_{AB} = (8k_B T/\pi\mu)^{1/2}$ is the mean interatomic velocity, $T(\omega, I)$ is $T(\omega)$ for intensity I, and $[A(i)]$ and $[B(i_1)]$ are the initial-state densities.

To obtain solutions of Eqs. (6) and (7), Eqs. (3a) and (3b) are used in (3c), which is then used in (4) to obtain $P(b, v, \omega)$. Equation (5b) and the solution of Eq. (4) are then substituted into (5a) to obtain $T(\omega)$ for Eqs. (6) and (7). This procedure is carried out in the Appendix.

The transitions that have been studied [e.g., Eqs. (1a), (1b), and (2a)] are those in which $|\Delta L| \leq 2$ on each atom. As the generalization from this restriction is straightforward but time consuming, we will limit most of the discussion to this condition. The form of the process in Eq. (1) being considered is then

$$A(n, L, S, J) + B(n_1) \rightarrow A(n', L \pm \Delta, S, J') + B(n_1) \pm \hbar\omega , \quad (1')$$

where $\Delta = 0$ or 2. This is induced by $V_r(t)$ plus the V_{qd} part of V' as indicated in the Eq. (1b′) example, with the result that the transition moment $\vec{D}(R)$ is proportional to R^{-4}. The $\Delta = 0$, $L = 0$ case (an $ns \rightarrow n's$ transition) is an exception which can only be induced by $V_r(t)$ between the mixed-in portions of both $\langle \alpha M M_1|$ and $|\alpha' M' M_1'\rangle$ in Eq. (4), equivalent to successive application of V_{dd}, V_r, and V_{qd}. This is necessary since the matrix element of all the multipole operators is zero between two s states. Thus $\vec{D}(R) \propto R^{-7}$ for the $ns \rightarrow n's$ case.

The form of the process in Eq. (2) being considered here is

$$A(n, L, S, J) + B(n_1, L_1, S_1, J_1) \rightarrow A(n', L \pm \Delta, S, J') + B(n_1', L_1 \pm \Delta_1, S_1, J_1') \pm \hbar\omega . \quad (2')$$

As indicated in the Eq. (2a′) example this transition is induced by the V_{dd} part of V' for the case $\Delta = 1, \Delta_1 = 0$ or 2, so that $\vec{D}(R) \propto R^{-3}$. ($V_{qq}$ can also yield a small contribution for some L, L_1, $\Delta = 1$, $\Delta_1 = 2$ cases.) It is induced by the V_{qd} part of the V' for cases $\Delta = \Delta_1 = 1$ and $\Delta = 0$, $\Delta_1 = 0$ or 2 resulting in $\vec{D}(R) \propto R^{-4}$. The exception is again the $nS \rightarrow n'S$ transition on either atom, which requires two applications of V' and one of $V_r(t)$, resulting in $\vec{D}(R) \propto R^{-6}(R^{-7})$ for the $V_{dd}(V_{qd})$ case. We will show that almost all the $\vec{D}(R) \propto R^{-n}$ cases with a particular n will have nearly the same characteristic line shape for small $|\omega - \omega_0|$, with certain exceptions that will be described below. Since the dipole radiation operator connects product states of opposite parity, the V_{dd} case applies to transitions in which the total parity of atoms A and B changes, and vice versa in the V_{dq} case. This can be a convenient bookkeeping aid.

D. Quasistatic wing

Before obtaining general solutions to Eqs. (3)–(7), considerable insight can be gained by considering the $|\omega - \omega_0| \gg 1/\tau_c$ limit, for which the stationary phase solution of Eq. (4) yields the quasistatic intensity distribution. [That Eqs. (3)–(7) reduce to this approximate result is verified in the Appendix below Eq. (A11).] The quasistatic theory[12,16,17] predicts an absorption coefficient at frequency ν in the line wing of the α to α' transition given, for negligible excited-state population and $\omega = 2\pi\nu = 2\pi c/\lambda$, by

$$k_\nu = [A(n)][B(n_1)] \frac{4\pi^2}{3\lambda\hbar g_n g_{n_1}} \times \sum_{MM'M_1M_1'} |\vec{D}[R(\nu)]|^2 \left(\frac{4\pi R^2}{|d\nu/dR|}\right)_{R(\nu)} \times e^{-\Delta V[R(\nu)]/k_B T} , \quad (8)$$

where $g_n = (2J_n + 1)$, $R(\nu) \equiv R_{MM_1}^{M'M_1'}(\nu)$ is obtained from $\hbar\nu = V_{\alpha' M' M_1'}(R) - V_{\alpha M M_1}(R) \equiv \Delta V(R)$, and $\vec{D}(R) = \langle \alpha M M_1(R)|e\vec{r}|\alpha' M' M_1'(R)\rangle$ is the transition-dipole moment. Equation (8) is a sum over final and average over initial molecular states which can contribute to the line profile, combined with the usual quasistatic assumption that the photon energy due to a transition at separation R is given by the potential difference at R. The $\exp(-\Delta V/k_B T)$

factor in Eq. (8) is part of the interatomic distribution function[16]; for $|h(\nu-\nu_0)| \ll kT$ it is normally about 1 and we will generally delete it below. The straight-line collision path assumption used for the line-core calculation forces this factor to equal 1.[17]

In most cases,

$$V_{\alpha MM_1}(R) - V_{\alpha MM_1}(\infty) \cong C_{\alpha MM_1} R^{-6} \tag{9}$$

in the large-R region responsible for the line shapes under investigation. ($C_{\alpha MM_1}$ is evaluated in the Appendix.) Thus $h[\nu_{MM_1}^{MM_1'}(R) - \nu_0] = (C_{\alpha MM} - C_{\alpha M'M_1'})R^{-6}$ and $R_{MM_1}^{M'M_1'}(\nu) = [(C_{\alpha MM_1} - C_{\alpha' M' M_1'})/h(\nu-\nu_0)]^{1/6}$. Taking $|\vec{D}(R)| = D_{\alpha MM_1}^{\alpha' M' M_1'} R^{-P}$, where the constant $D_{\alpha MM_1}^{\alpha' M' M_1'}$ will be given below Eq. (20), and deleting the exponential factor Eq. (8) becomes

$$\frac{k_\nu}{[A(n)][B(n_1)]} = \frac{16\pi^4}{9\lambda g_n g_{n_1}} \times \sum \frac{|D_{\alpha MM_1}^{\alpha' M' M_1'}|^2}{|C_{\alpha MM_1} - C_{\alpha' M' M_1'}|} \times \left(\frac{C_{\alpha MM_1} - C_{\alpha' M' M_1'}}{h(\nu-\nu_0)}\right)^{(9-2P)/6}. \tag{10}$$

The quasistatic absorption coefficient of Eq. (8) applies when $|\nu-\nu_0| \gg 1/2\pi\tau_c$ on the "static" wing; that for which $h\nu = V_{\alpha MM_1}(R) - V_{\alpha' M' M_1'}(R)$ for each combination of M values. The absorption coefficient of Eq. (10) requires the additional validity of Eq. (9) and $D \propto R^{-P}$. If Eq. (9) is valid at $R > R_m$, where this defines R_m and $\hbar\omega(R_m) = V_{\alpha' M' M_1'}(R_m) - V_{\alpha MM_1}(R_m)$, then Eq. (10) applies to the wing region $\tau_c^{-1} < |\omega-\omega_0| < |\omega(R_m)-\omega_0|$. As will be noted in the examples below, the $V(R)$ usually differ from Eq. (9) before they change from $V(\infty)$ by even 10 cm^{-1}. Thus Eq. (10) generally loses validity at $|k-k_0| > 10$ cm^{-1}, where $2\pi ck = \omega$ and $2\pi ck_0 = \omega_0$. Nonetheless we use it in most of the examples below even in the $|k-k_0| > 10$ cm^{-1} region since it represents the leading term for the general case, while the correction is specific to each case and usually uncertain.

In Eq. (10) the static wing is that for which the term inside the parentheses of Eq. (10) is positive. Thus if $C_{\alpha' MM_1'} - C_{\alpha MM_1}$ is positive, corresponding to an increasing separation of the molecular potentials, it applies on the positive $\nu-\nu_0$ (blue) wing, and vice versa. If some $C_{\alpha MM_1} - C_{\alpha' M' M_1'}$ combinations are positive and others negative, both wings will have such quasistatic contributions. If $C_{\alpha MM_1} - C_{\alpha' M' M_1'}$ have the same sign for all M, M_1, M', and M_1' the static wing will be much stronger than the other "antistatic" wing, with the latter expected to be exponentially small for $|\nu-\nu_0| \gg 1/2\pi\tau_c$. Examples of these line shapes and the successes and inadequacies of the approximations are given in the comparisons to experiment in Sec. III.

For the transitions of Eqs. (1′) or (2′) without a change in total parity, $P=4$ in Eq. (10) and the quasistatic wing falls off as $|\nu-\nu_0|^{-1/6}$. For the transition in Eq. (2′) which changes the total parity $P=3$ and the quasistatic wing falls off as $|\nu-\nu_0|^{-1/2}$. For the case of an $nS \rightarrow n'S$ transition on either atom, $P \geq 6$ and the quasistatic wing increases at least as rapidly as $(\nu-\nu_0)^{1/2}$. Thus in the $nS \rightarrow n'S$ case we typically expect a broad molecular band which terminates in the neighborhood of ν_0, with only a weak electric quadrupole line proportional to $[A(n)]$ at ν_0 for the class of transitions in Eq. (1). This type of behavior is generally, but not always, seen in the $nS \rightarrow (n+1)S$ transitions of the alkalis reported in Ref. 5. We will not evaluate the line core ($|\omega-\omega_0| < 1/\tau_c$) portion of the line for this $S \rightarrow S$ case as it is very weak according to the present theory. For the other cases we expect k_ν or I_ν to be peaked near ν_0 and decrease rapidly on the antistatic wing. Note that the $\Delta=3$ case in Eqs. (1′) or (2′) would result in $P=5$ and the band should be observable to ν_0. For $\Delta \geq 4$, $P \geq 6$ and again very little intensity is predicted at ν_0.

E. Line core

The line-core shape results from Eq. (3) in (4), which is then substituted into (5) and (6). The details of this calculation are given in the Appendix, and we will only outline the salient points and results here.

We evaluate the $|\alpha MM_1(R)\rangle$ of Eq. (3a) and $V_{\alpha MM_1}(R)$ of (3b) in the molecular-axis reference frame. We retain only the leading C_6R^{-6} term in the interaction potential of Eq. (3a), but include its M dependence. For the parity conserving (or changing) transitions we retain in Eq. (3b) only the states mixed in by the V_{dd} (or $V_{dq}+V_{qd}$) interaction, as these are the dominant terms responsible for the induced transition moment. The rotation of the radiation field relative to the molecular axis during a collision is then included in the $V_r(t)$ radiation perturbation [Eqs. (A7) and (A8)]. After averaging over collision-frame angles, we obtain a single-collision line shape [Eq. (A8)], in terms of a sum over initial and final M states of line-shape functions $|Z(\cdots)|^2$, weighted by M-dependent terms $|F(\cdots)|^2$. The sum also extends over three separate line-shape terms $q=-1,0,1$, corresponding to $U_q=1$, $\cos\theta(t)$, and $\sin\theta(t)$ terms in the $Z(\cdots)$ time integral, where $\theta(t)$ is the rotating angle of the molecular axis during the collision (see Fig. 3). Except for these rotation terms, the $Z(\cdots)$ time integral is very similar to that in Eq. (3b′).

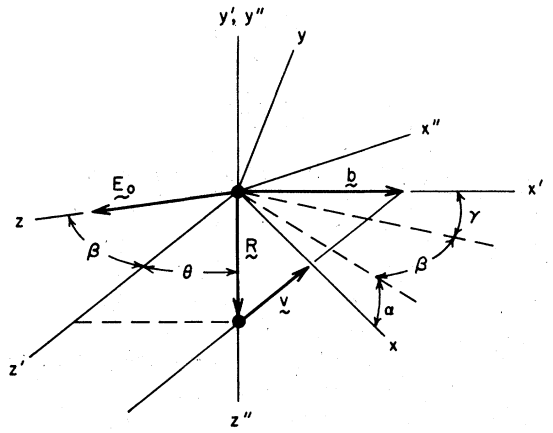

FIG. 3. Rotation of the unprimed laboratory axes through Euler angles α, β, γ to the primed collision frame, and then through Euler angles 0, $\theta(t)$, 0 to the rotating, double-primed frame.

The single-collision line shapes are averaged over impact parameter b and impact velocity v, Eq. (A10). Combining Eq. (A10) with Eq. (6) yields the general result for the absorption coefficient:

$$k_\nu = \frac{16\pi^{3/2}(e^2/\hbar c)\omega}{v_0(C/\hbar v_0)^{2I/5} g_n g_{n_1}} \times \sum_{\substack{mq \\ MM'M_1M_1'}} \left| \sum_{kk_1} F(\cdots) \right|^2 a_{qm} L(D, l, U_q). \quad (11)$$

Here the $L(D, l, U_q)$ are line-shape functions with magnitude ~1 at $\omega - \omega_0 = 0$; they are expressed in terms of a dimensionless frequency variable $D = (\omega - \omega_0)(C/\hbar v_0)^{1/5}/v_0 \equiv (\omega - \omega_0)\tau_c$, where τ_c is the "collision time" discussed in Sec. II F. These $L(D, l, U_q)$ for $q = 1, 0, -1$ are given in Table I and Fig. 4(a) for the $l = 1$ (V_{dd}-induced) case, and in Table I and Fig. 4(b) for $l = 2$ (V_{dq}-induced) case.

TABLE I. $L(D, l, U_q)$ of Eq. (A10).

D	$l=1$ $q=-1$	$l=1$ $q=0$	$l=1$ $q=1$	$l=2$ $q=-1$	$l=2$ $q=0$	$l=2$ $q=1$
3	0.54	0.35	0.17	0.75	0.495	0.235
2	0.64	0.42	0.21	0.77	0.505	0.24
1	0.88	0.56	0.26	0.79	0.51	0.22
0.5	1.08	0.68	0.28	0.77	0.49	0.20
0.25	1.22	0.74	0.28	0.74	0.47	0.185
0.0	1.36	0.78	0.27	0.65	0.41	0.17
−0.25	0.80	0.54	0.25	0.50	0.33	0.15
−0.5	0.50	0.38	0.22	0.36	0.26	0.135
−1	0.22	0.18	0.13	0.20	0.16	0.10
−2	0.058	0.054	0.048	0.058	0.057	0.045
−3	0.019	0.018	0.018	0.026	0.024	0.022
−4	0.008	0.007	0.007	...	...	...

The complete $l = 1$ (or 2) line shapes will be given, from Eq. (11), by q-weighted sums of these three $L(D, l, U_q)$ functions. The relative weighting comes from the $|F(\cdots)|^2$ factor, summed over M values, and the a_{qm} fraction which results from the angular average discussed below Eq. (A8). The sum over $m = 0, \pm 1$ comes from the projection of the three independent polarizations onto the electric vector of the incident radiation field (assumed linearly polarized). The relative weight assigned to each of the three $L(D, l, U_q)$ line shapes thus depends on the particular L or J values of the atomic states involved in the $\alpha \to \alpha'$ transition. Furthermore, the $\omega - \omega_0$ scale is given by $\omega - \omega_0 = Dv_0/(C/\hbar v_0)^{1/5}$, where $C \equiv C_{\alpha' M' M_1'} - C_{\alpha M M_1}$ is different for different contributions. Thus there is no single universal line shape for all V_{dd}- (or V_{dq}-) induced transitions. Equation (11) covers all $\Delta L \leq 2$ cases of type-1 and type-2 line shapes. The

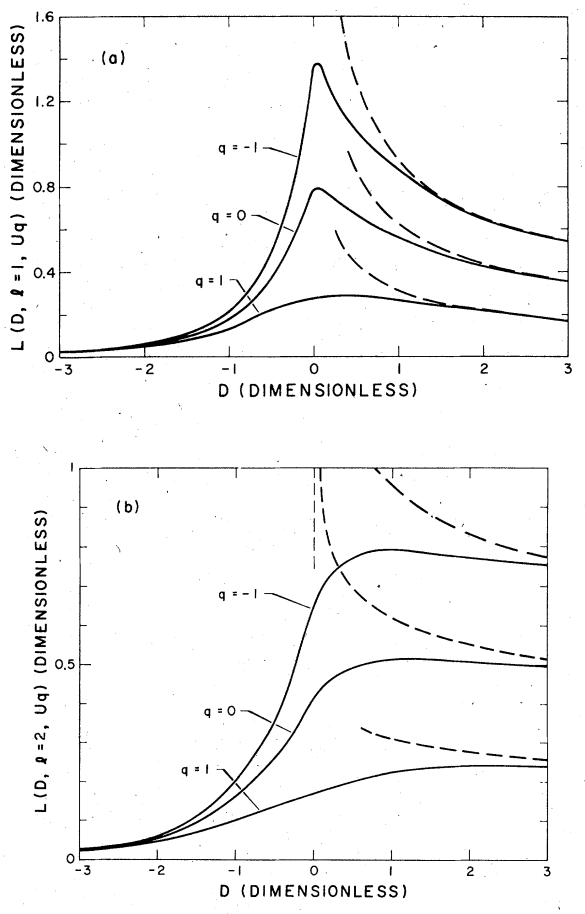

FIG. 4. Dimensionless line-shape function $L(D, l, U_q)$ for the $l = 1$ case (a) and $l = 2$ case (b). The parameters are defined in Sec. II E and Eq. (A10). This converges to the quasistatic limit (dashed lines) at large positive D.

three additional $L(D, l, U_q)$ functions for $\Delta L = 3$ can be obtained by obvious extension of the formulas, while $\Delta L > 3$ yields negligible intensity near ω_0.

The sum over M's and $m = 0, \pm 1$ in Eq. (11) or (A10) does not reduce to a simple form due to the M dependence of C in the $L(D, l, U_q)$. It can be simplified considerably by using an M-averaged $\overline{C}$ in $L(D, l, U_q)$. A further approximation, equivalent to ignoring the molecular axis rotation, is to use only the $U_q = 1$ or $q = -1$ line shape, properly weighted as given above Eq. (A11). A much simpler approximation to the line core shape results [Eq. (A11)]. The accuracy of this approximation will be noted in the following examples.

These general equations (A10) and (A11) are reduced in the Appendix to expressions for k_ν [Eqs. (A12) and (A16)] for the (class 1, $l = 2$) case of $nS \rightarrow nD$ transitions of atom A with atom B an $L = 0$ ground state atom, as in the examples of Eqs. (1a) and (1b). Next, Eqs. (A10) and (A11) are reduced in the Appendix to Eqs. (A18) and (A19) for the case of a (class 2) "radiative collision" in which $\Delta L = 1$ for atom A and $\Delta L = 2$ for atom B. This will be applied to the $Sr^* + Ca \rightarrow Sr + Ca^*$ problem in Sec. III.

F. Stationary-phase limit

For positive $(\omega - \omega_0)/C$, the argument of the exponential in Eq. (A9) can be expanded as a quadratic about the stationary phase point x_S. The resulting stationary phase solution for Z yields $3L(D, l, q = 1) = 1.5L(D, l, q = 0) = L(D, l, q = -1) = \frac{1}{6}\pi^{3/2} D^{(2l-5)/6}$ in Eq. (A10). Then Eq. (A10) yields, with Eq. (6), the quasistatic wing intensity given in Eq. (10) where $P = l + 2$, $m = M_1 - M_1' + M - M'$, and

$$\left| D^{\alpha' M' M_1'}_{\alpha M M_1} \right|^2 = \left| F(nMn_1M_1, n'M'n_1'M_1'; ml) \right|^2 . \quad (12)$$

The exponential factor is missing in this quasistatic limit of Eq. (A10) because we have assumed straight-line paths. That this relation should hold is apparent from comparing the definition of $F(\cdots)$ below Eq. (A8) to Eq. (A5) or (A6) and noting the identification of $D^{\alpha' M' M_1'}_{\alpha M M_1}$ below Eq. (8) as the transition dipole moment. These stationary-phase limits to the $L(D, l, U_q)$ are given as dashed lines in Fig. 4. It can be seen there that the exact line shapes converge to this limit in the neighborhood of $D = 1$. These stationary-phase limits are the foundation of the quasistatic approximation, so the agreement is not accidental.

The exact solution [Eq. (A10)] thus converges to the quasistatic limit [Eq. (10)] for $D \gg 1$, with the transition from the quasistatic to "dynamical" portion of the line at $D \cong 1$. This corresponds to $|\omega - \omega_0| = v_0/(C/\hbar v_0)^{1/5}$, as could have been predicted by dimensional analysis. This transition frequency is the same as the transition frequency between the quasistatic and impact limits for allowed-dipole transitions in a CR^{-6} difference potential.[19] This transition frequency is generally called the Weisskopf frequency, and its inverse is often identified as "τ_c," the characteristic "collision duration time."

III. COMPARISONS TO DATA

A. Class 1

The only data we are aware of for class 1 collisions are for $nS \rightarrow n'D$ transitions of atom A, with atom B in an S state. The following cases have been measured.

Cs-Xe

Equations (A12)–(A15) have been used to obtain k_ν for the Cs $6\,^2S \rightarrow 5\,^2D_j$ and $6\,^2S \rightarrow 6\,^2D_J$ absorption coefficients due to Xe. In Fig. 5 the line-center shapes for $6\,^2D_{5/2}$ and $6\,^2D_{3/2}$ are given, and the approximation of Eq. (A11) as given in Eq. (A16) (long-dashed line in Fig. 5) is also given for the $J = \frac{5}{2}$ case. This approximation uses

$$\overline{C} = \alpha_{Xe}(\langle r^2_{n'D} \rangle - \langle r^2_{nS} \rangle)$$

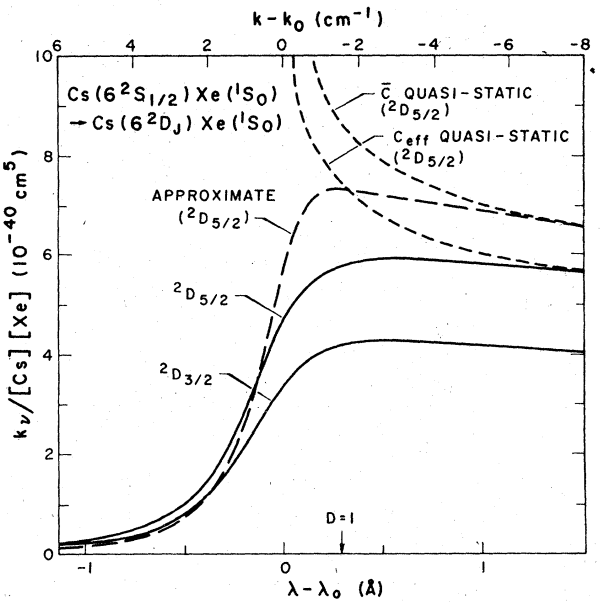

FIG. 5. Theoretical coefficients for $Cs(6\,^2S_{1/2} \rightarrow 6\,^2D_J)$ absorption in the presence of Xe. For the $J = \frac{5}{2}$ case the more-exact theory (solid line) is compared to the quasistatic limit using an effective C(short-dashed line), and to the approximation of Eqs. (A11) and (A17) (long dashed line). This describes the $6\,^2S_{1/2} \rightarrow 5\,^2D_J$ absorption as well if the k_ν scale is multiplied by 32 and the $k - k_0$ scale by 1.70 (see text).

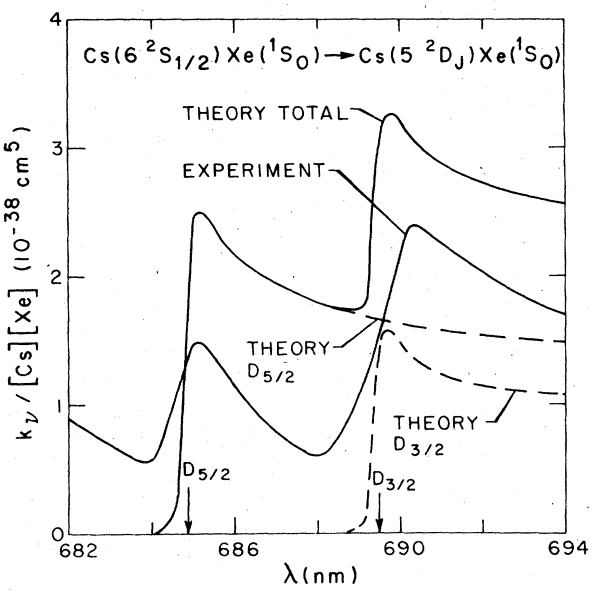

FIG. 6. $Cs(6\,^2S_{1/2} \rightarrow 5\,^2D_J)$ absorption coefficient due to Xe as calculated and as measured by Moe *et al*. (Ref. 5) at [Xe] $\cong 10^{20}/cm^3$. The intensity measured at $\lambda \leq 684$ nm is the beginning of a band that dominates the spectrum. It is attributed to a transition to the strongly repulsive $\Omega = \frac{1}{2}$ molecular adiabatic state, associated with $Cs(5\,^2D)Xe(^1S_0)$ separated limit.

from Eq. (A15), underestimating the effective C_6 for the D state because smaller M values have larger transition moments and larger C_6 coefficients. The line shape in Fig. 5 also applies to the $6\,^2S_{1/2} \rightarrow 5\,^2D_J$ absorption coefficient if the k_ν scale is multiplied by 32 and the $k - k_0$ scale by 1.70. This results because changing from $6\,^2D$ to $5\,^2D$ only affects the size of $\mathcal{R}_{nL,n'L'}$ and of C in Eqs. (A12)–(A15).

The absorption coefficients to $5\,^2D_J$ and $6\,^2D_J$ are compared to experiments in Figs. 6 and 7. We have used $\mathcal{R}_{nS,n'D} = 24a_0^2$ for $n = 5$ and $16a_0^2$ for $n = 6$, obtained from Ref. 6. (In cases without experimental data, Ref. 20 gives a Coulomb approximation for $R_{nS,n'D}$.) The absolute absorption coefficient measurements of Ref. 5 are extremely valuable for these comparisons, as there are no adjustable terms. This comparison indicates that the present approximations are fairly good for the $5\,^2D_J$ states, particularly since the experimental data are somewhat broadened by high Xe density and experimental resolution. The theoretical profiles will drop more rapidly with increasing $\lambda - \lambda_0$, as in the experimental data, when the R^{-8} and higher terms are included in $V(R)$, i.e., $|d\nu/dR|^{-1}$ in Eq. (8) decreases with increasing $|\nu - \nu_0|$, corresponding to smaller R. Note also, that Eq. (A16) predicts $|k_\nu| \propto (\alpha_B)^{1.2}$, which is consistent with the results in Fig. 5 of Ref. 5.

The two measurements of the $6\,^2S_{1/2}$-$6\,^2D_J$ absorption coefficient, shown in Fig. 7, can be reconciled by noting that the [Xe] = 4 amagat (1 amagat = $2.7 \times 10^{19}/cm^3$) measurements of Moe, Tam, and Happer[5] are reasonably consistent with a broadened form of the lower-pressure Kielkopf-Gwinn measurements.[2] Thus if the latter, relative measurements are normalized to the former as indicated in Fig. 7, they probably represent the low-pressure normalized line shape. The theoretical profile compares very poorly to this, both

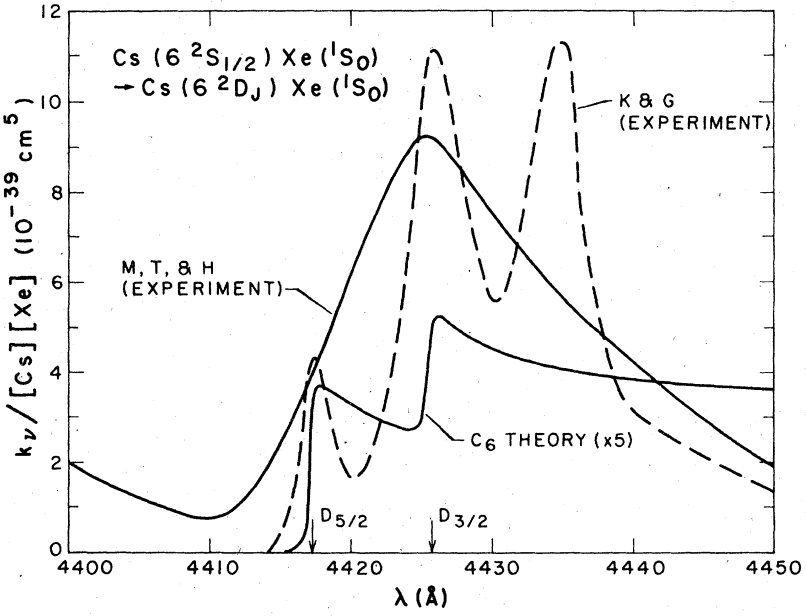

FIG. 7. $Cs(6\,^2S_{1/2}$-$6\,^2D_J)$ absorption coefficient due to Xe as calculated, as measured by Moe *et al*. (Ref. 5) in absolute units at [Xe] $= 10^{20}/cm^3$, and as measured by Gwinn *et al*. (Ref. 2) at much lower [Xe]. The latter measurements were in relative units and have been arbitrarily normalized.

in magnitude and shape. The difference in magnitude, the rapid drop of the experimental red wings, and nonstatistical $D_{3/2}$:$D_{5/2}$ intensity ratio implies that for the $\alpha' = 6^2D_J$ states the $\Delta V = C_{\alpha' M' 0} R^{-6}$ assumption of the present, small $|\nu - \nu_0|$ theory breaks down at quite small $|\nu - \nu_0|$, invalidating the theory. This is also indicated by the scaling of $|k_\nu|$ for different noble gases in Fig. 6 of Ref. 5, which does not follow $(\alpha_B)^{1.2}$.

In these examples we expect fine-structure recoupling (change of Hund's case c to case a) to occur when $\hbar|\Delta\omega|$ is comparable to the fine-structure energy $\Delta E_{\rm FS}$. The effect of this on ^2D_J energy levels has been given by Nikitin[21] and the effect on the Cs-Cs spectrum by Niemax.[6] It is also apparent in the Cs(5 ^2D)-Xe potentials calculated by Pascale and Vandeplanque (Fig. 1),[22] in the red satellite in Fig. 7, and in the strong blue-wing bands in Ref. 5, which are attributed to a Σ level that is weakly attractive at large R but becomes strongly repulsive at small R. The simple long-range approximation of the present theory does not describe any of these effects, and can only be applied across a range of $\hbar|\Delta\omega| \ll \Delta E_{\rm FS}$. In the Cs($6\,^2S_{1/2} - 5\,^2D_J$) case, $\Delta E_{\rm FS} \gg \hbar/\tau_c$, and our assumed $V_{\alpha' M' 0}(R)$ are fairly accurate for $\omega - \omega_0 \leq 1/\tau_c$, yielding reasonable fits to the experimental k_ν in the neighborhood of each fine-structure line. In the Cs($6\,^2S_{1/2} - 6\,^2D_J$) case $\Delta E_{\rm FS} \sim \hbar\tau_c^{-1}$, severe departures from the assumed $V_{\alpha' M' 0}(R)$ occur within the core of the lines ($\omega - \omega_0 \leq \tau_c^{-1}$), and very poor agreement is obtained. Kielkopf[23] as well as Pascale and Vandeplanque[22] have provided sets of potentials for the $6\,^2D_J$ and $6\,^2S_{1/2}$ states. These could be combined with the M-dependent transition moments of the present theory to obtain improved theoretical predictions, but this is beyond the scope of the present paper. If the fine-structure splitting $\Delta E_{\rm FS} < \hbar/\tau_c$ (which does not hold for Cs) fine structure can be ignored and the present theory applies until the long-range approximations break down for other reasons such as proximity to other levels, $C_8 R^{-8}$ terms, and repulsive terms in $V^*(R)$.

Cs-Cs

The Cs $6\,^2S$-$5\,^2D_J$ transition due to Cs collisions has been measured with very high resolution, and in absolute units.[6] For this particular transition, the approximations for $f(E)$ below Eq. (A13) and the similar energy approximation used to obtain Eq. (A16) are inaccurate by almost a factor of 3 and must be replaced by the actual atomic-state energies. In Fig. 8 we compare the evaluation of Eqs. (A12), (A13), and (A15) to this k_ν data. As in the above Cs($6^2S_{1/2}$)Xe($^1S_0$) $\rightarrow$ Cs(5 ^2D) Xe($^1S_0$) case, $\Delta E_{\rm FS} \gg \hbar\tau_c^{-1}$ and the assumptions of the present theory appear to correctly represent many features of the observations. Again, this comparison is on an absolute scale, with no adjustable parameters.

O-Ar

The oxygen ^1S-to-^1D transition collisionally induced by a noble gas has received considerable attention recently due to its potential as a high-power excimer laser and/or gain cell (see Refs. 3 and 4 and references therein). The spectrum of O-Ar has been calculated in Ref. 4, using the long-range dipole-quadrupole interaction to fix the transition moment. Our model uses the same transition moment [$F(\cdots)/R^4$, with $F(\cdots)$ given by Eq. (A14)], but our assumption $V^*(R) - V(R) = (C_{\alpha' 00} - C_{\alpha M0}) R^{-6}$ is exceedingly inaccurate for this case. The $C_{\alpha' 00}$ and $C_{\alpha M0}$ Van der Waals coefficients are nearly identical for this transition between $\alpha' = {}^1S_0$ and $\alpha = {}^1D_2$ states of the same configuration, whereas the $^1D_2$ state has a $C_{8M} R^{-8}$ interaction that is not balanced in the ^1S state.[4] Thus in the $R = 8$–$12 a_0$

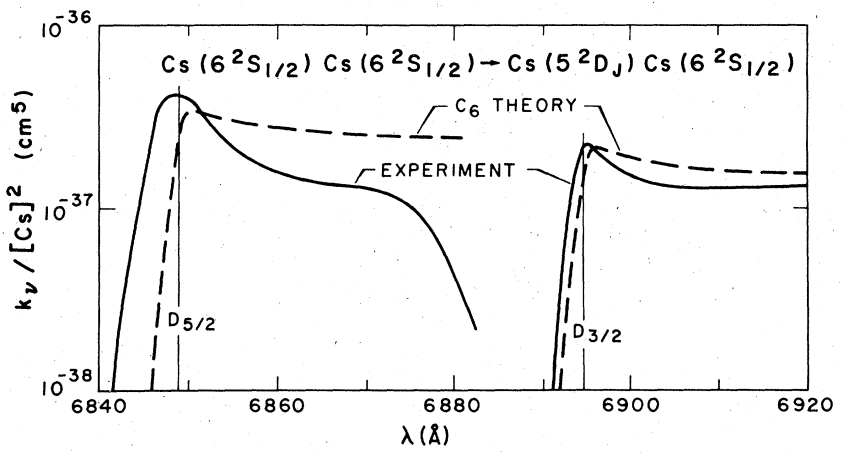

FIG. 8. Cs($6\,^2S_{1/2}$-$6\,^2D_J$) absorption coefficient due to Cs collisions. The theory, using only $C_{JM} R^{-6}$ potentials, is compared to the measurements of Niemax (Ref. 23). The measurements and theory are in absolute units.

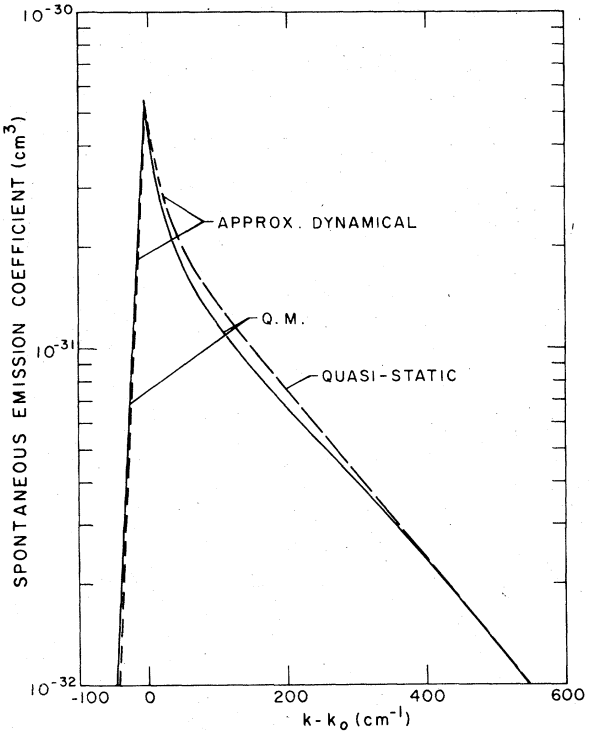

FIG. 9. Spontaneous emission coefficients ([Xe][O(^1S)] $\times 8\pi/\lambda^2$ times the stimulated emission coefficient) for O($^1S\Sigma$)→O($^1D\Sigma$) in the presence of Xe at 300 K. The quasistatic theory (long dashes) and present approximate dynamical theory (short dashes) utilize the potentials and transition moment given in Ref. 4. Inclusion of quasibound $^1S\Sigma$ states in the quantum mechanical calculation of Ref. 4 (solid line) is expected to remove the small discrepancy in the 20–200-cm^{-1} region.

region responsible for the line core and near wings, the various $V^*(R) - V(R)$ are predominantly due to attractive R^{-8} terms and repulsive overlap terms.

The quasistatic theory in Eq. (8) applies to any potentials, whereas the line-core shapes of Sec. II E are specific to C_6R^{-6} interactions and are not applicable here. Nonetheless, one can estimate that the result of applying the present line-core theory to $V^*(R) - V(R) \propto R^{-8}$ and a transition moment $D(R)^2 \propto R^{-8}$ would resemble the $U_q = 1$ curve in Fig. 4(a) since this applies to $D(R)^2 \propto R^{-6}$, $V^*(R) - V(R) \propto R^{-6}$. The transition to the quasistatic wing then occurs at $D = 1$ or $|k - k_0| = h^{-1}c^{-1}v_0[(C_8^* - C_8)/hv_0]^{-1/7} \cong 13$ cm^{-1} for the O(S_0) Ar → O($^1D_{2,M}$) Ar transition at 300 K. In Fig. 9 the O-Ar quasistatic spectrum for the dominant $M = 0$ term (labeled $2\Sigma \rightarrow 1\Sigma$ in Ref. 4) is calculated using the potentials of Ref. 4 in our Eq. (8). A short dashed line indicates the Eq. (A11) approximation for the line-core and antistatic (red) wing behavior. For comparison the $2\Sigma - 1\Sigma$ spectrum reported in Ref. 4, obtained from Franck-Condon factor calculations using the same transition moments and potentials, is shown in Fig. 9. In the 50–250-cm^{-1} region the quasistatic spectrum is about 15% larger than the quantum-mechanical spectrum of Ref. 4 due to the omission of quasibound-state contributions in the latter calculation. When these are included[24] the quantum results oscillate only a few percent above and below the present quasistatic spectrum for $|k - k_\nu| > 20$ cm^{-1}, as we expect for molecular bands which average over many vibrational and rotational states. Thus the present theory accurately fits these very complete calculations. This supports our supposition that the above disagreements between the experimental and theoretical k_ν (for Cs-Xe and Cs-Cs) are primarily due to departures of $V^*(R)$ and $V(R)$ from the assumed long-range form. Comparisons to experimental O-Ar spectra are made in Ref. 4, so are not discussed here.

The present calculations have ignored the M mixing by the nuclear axis rotation. Consequently we obtain transition moments $F(\cdots)/R^4$ which connect the O ^1S state only to the $^1D_{2,M}$ state with $M = 0, \pm 1$ [see Eq. (A14)]. In Ref. 4 an equivalent assumption was made by the use of Hund's coupling scheme (a) to describe the ^1D states as $^1\Sigma$, $^1\Pi$, and $^1\Delta$ states. For thermal collisions of O-Ar, the rotational-mixing perturbation between $^1D_{2,1}$ and $^1D_{2,2}$ state is comparable to their ~10-cm^{-1} splitting at $R = 7-8a_0$. This mixes the wave functions and thereby the transition moments. The effect of such mixing will often largely average out of the final spectrum, but in this case $V^*(R) - V(R)$ exceeds $h\nu_0$ for the $^1D_{2,0}$ and $^1D_{2,\pm1}$ states but falls below $h\nu_0$ for the $^1D_{2,\pm2}$ states. Thus the rotationally induced transition moment to the $^1D_{2,\pm2}$ states contributes "quasistatic" intensity on the red wing. Since the above theory without inclusion of this mixing predicted quasistatic intensity only on the blue wing and an exponential decrease on the red wing, this causes a major increase in the red-wing intensity. This effect is being treated very thoroughly by the authors of Ref. 4,[24] so we will not discuss it further here.

B. Class 2—"Radiative collisions"

The only line-shape measurement is that of Falcone *et al.*[9] on the Sr($5\,^1P_1$)Ca($4\,^1S_0$) → Sr($5\,^1S_0$)Ca($6\,^1S_0$) transition at 497.7 nm. Since a D final state of Ca is a somewhat different case that may be measured soon, we also include it. The absorption coefficients, or equivalent cross sections obtained with Eq. (A18) or (A19) in Eq. (6) or (7), are given in Figs. 10 and 11 for the cases of $6\,^1S$ and $5\,^1D$ final states on Ca. For these cases 80% of the transition moment comes from the $k_1 = 4$ term in Eq. (A18), for which fairly relia-

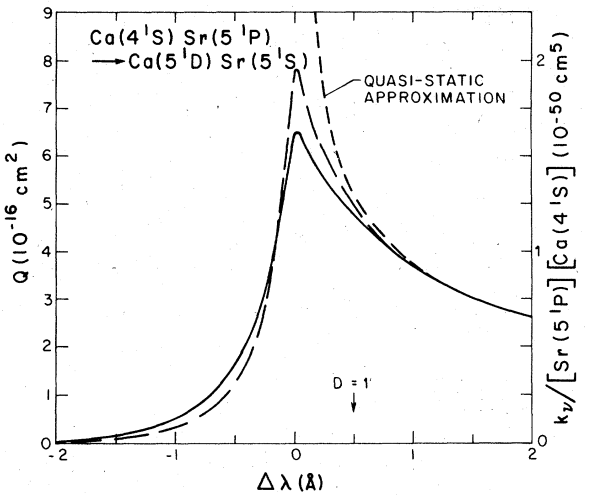

FIG. 10. Absorption coefficient, or collision cross section at 1-MW/cm^2 light intensity, for the $Ca(4\,^1S)Sr(5\,^1P) \rightarrow Ca(5\,^1D)Sr(5\,^1S)$ transition at $\lambda_0 = 471.1$ nm. The long-dashed line is the approximation of Eq. (A19); the solid line is the more exact (A18).

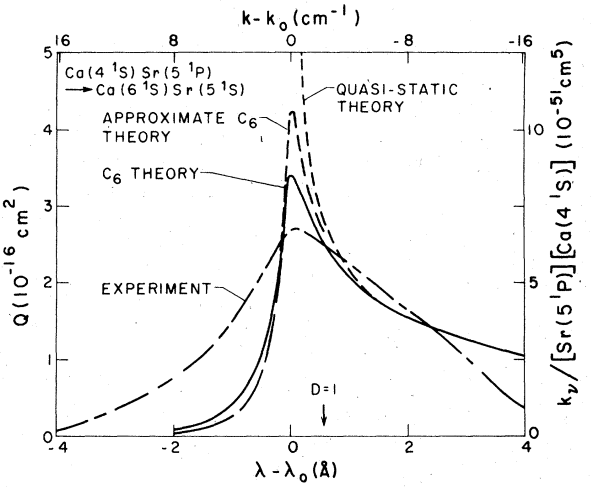

FIG. 11. Absorption coefficient, or collision cross section at 1-MW/cm^2 light intensity, for the $Ca(4\,^1S)Sr(5\,^1P) \rightarrow Ca(6\,^1S)Sr(5\,^1S)$ transition at $\lambda_0 = 497.7$ nm. The experimental measurement of Ref. 9 has been normalized to the theory.

ble $\mathcal{R}$ values are available (Table II). The approximation of Eq. (A19) is compared to the more exact Eq. (A18), which includes the molecular axis rotation. The measured line shape for the $6\,^1S$ state case, from Ref. 9, is compared to the calculations in Fig. 11. The measurements which yielded a lower bound of 2×10^{-17} cm^2 at 1-MW/cm^2 laser power have been normalized to the theory, as it would be expected to appear in the peak region if broadened by the ~2-cm^{-1} laser linewidth in the experiment. The more rapid drop in the measured cross section at $\lambda - \lambda_0 > 2$ Å is expected to be due to the C_8R^{-8} and higher terms in the $Ca(6\,^1S)$-$Sr(5\,^1S)$ interaction potential, which could readily be incorporated into the quasistatic theory [Eq. (8)]. However, the present theory fails to explain the intensity observed on the blue wing. This is not due to resonance broadening of the $Sr(5\,^1P)$ level, which is only 0.2-cm^{-1} full width at the experimental densities; also the broadening of $Ca(6\,^1S)$ is an order of magnitude smaller.

The theory given in Ref. 9 for the peak cross section for this process would yield quite similar results to the present Eq. (19) approximation if the energy shifts ($C_6^*R^{-6}$) of the $Sr(5\,^1S)Ca(6\,^1S)$ final state were included in their calculation. However, the calculated cross sections and equations in Ref. 9 include only the energy shift (C_6R^{-6}) of the $Sr(5\,^1P)Ca(4\,^1S)$ state. Since $C_6^* \gg C_6$, the magnitude of the cross section and the sign of $\lambda - \lambda_0$ implied for the larger static wing (blue versus red-wing) are incorrect in Ref. 9. The original theory of Ref. 7 for this "radiative collision" process is also very similar to the present calculation [e.g., Eq. (2.1) of the second paper is equivalent to our Eq. (3b′) and their Eq. (2.7) is the quasistatic limit]. As noted in Sec. I, the present calculation

TABLE II. Calcium radial integrals $\mathcal{R}$.[a]

	$4\,^1S$ (0)	$5\,^1S$ (33 317)	$6\,^1S$ (41 786)	$7\,^1S$ (44 276)	$4\,^1D$ (37 298)	$4\,^1D'$ (40 720)	$5\,^1D$ (42 919)	$6\,^1D$ (44 940)
$4\,^1P$(23 652)[b]	4.94		3.05		0.9	4.1	2.65	1
$4\,^1P'$(36 731)	0.090	(1.1)	(4.1)	(–1.8)	(10.4)	(12)	(4.3)	(–2.8)
$5\,^1P$(41 679)	0.58	(2.2)	(21)	(6.7)	(3.6)	(14.6)	(21)	(4.5)
$6\,^1P$(43 933)	0.72	(–2.1)	(16)	(29)	(–1.2)	(2.9)	(17)	(28)
$7\,^1P$(45 425)	0.49	(1.0)	(–2.5)	(24)	···	(–1.7)	(~0)	(30)

[a] The integrals are in a_0 units. The value labeled T is from Ref. 25, the unlabeled values are from Ref. 26, and those in parentheses are from the Coulomb approximation. Of the latter, only the large values may be reliable.

[b] The energy of each level, in cm^{-1}, is given next to the assignment.

differs primarily by the inclusion of the molecular axis rotation, M degeneracy, and actual integration over b, v, and the collision time without introduction of cutoffs and approximations. The calculation of Ref. 10 does not include the effect of the R dependence of $V^*(R)$ and $V(R)$; thus it obtains a quite different low-intensity line shape than that of the present calculations.

IV. CONCLUSIONS

The present calculations represent the first general but quantitative theory of collisionally induced dipole-forbidden atomic transitions. It has utilized the concepts and methods of the traditional theory of line shapes for dipole-allowed transitions. As with the latter, failures of the present calculations are most often due to inaccuracies in the interatomic potentials used in the calculation. To avoid excessive detail at this stage in the theory, we have utilized only the leading long-range terms $C_{\alpha MM_1}R^{-6}$ for the potentials. The one exception is the O-Ar case where we utilized a set of theoretical potentials in order to make comparisons with the molecular spectra calculated by the more exact Franck-Condon factor theory. The favorable comparison obtained here is the best indication that the present theory correctly treats some aspects of the problems. As noted in that section, however, this case is an example of where our neglect of rotational mixing has a major effect on one wing, and both the present theory and Ref. 4 must be corrected for this in order to compare favorably with experimental spectra.

It is clear from the successes and failures in the above comparisons that the next round of improvement to this theory is to use improved potentials. This requires evaluation of R^{-8} and higher terms, repulsive terms, fine-structure recoupling, satellite and wing-shape data, and many forms of potential calculations. Every case must be treated on an individual basis, utilizing a full array of experimental and theoretical information to optimize the potentials. Except insofar as the transition moment may also differ significantly from its long-range form, this makes the present problem the same as that of interpreting the shapes of collisionally broadened allowed transitions.

ACKNOWLEDGMENTS

We wish to thank Chela Kunasz for careful numerical evaluation of the line-shape integrals. We also wish to thank Sydney Geltman, Jinx Cooper, John Carlsten, Steve Harris, James Young, and Paul Julienne for providing valuable ideas and comments.

APPENDIX: LINE-CORE CALCULATION

In evaluating Eq. (3) for $V' = V_{dd}$ or $V_{dq} + V_{qd}$ it is convenient to quantize all electronic states along the internuclear axis $\hat{R}$. This has the advantage of making the energies $V_{\alpha MM_1}(\vec{R})$ in Eq. (3b) depend only on R and the mixing in Eq. (3a) similarly depends only on R and is diagonal in the total electronic M_J of the product basis states. However, the radiation field $\vec{E}_0$ is along a fixed laboratory axis, so we will include below its effective rotation with respect to $\hat{R}$. For this quantization axis and $V_{dd} \equiv V_{11}$, $V_{qd} \equiv V_{21}$,[18]

$$V_{l1} = R^{-l-2}e^2 \sum_{\mu=0,\pm1} \frac{(-1)^l(l+1)!}{[(1-\mu)!(1+\mu)!(l-\mu)!(l+\mu)!]^{1/2}} \left(\frac{4\pi}{2l+1}\right)^{1/2} \mathcal{Y}_{l\mu}(r_A) \left(\frac{4\pi}{3}\right)^{1/2} \mathcal{Y}_{1-\mu}(r_B), \tag{A1}$$

where we use the notation $\mathcal{Y}_{l\mu}(r)$ [Eq. (5.1.2) of Ref. 27] for the spherical harmonics $M_l^{\mu}(r)$ of Ref. 18, and $(\frac{4}{3}\pi)^{1/2}\mathcal{Y}_{1\mu} = r_\mu$. We define

$$R^{-l-2}V(l)^{n'M',n_1'M_1'}_{nM,n_1M_1} \equiv \langle A(n,L,S,J,M)B(n_1,L_1,S_1,J_1,M_1)\,|\,V_{l1}\,|\,A(n',L',S,J',M')B(n_1',L_1',S_1,J_1',M_1')\rangle. \tag{A2}$$

Then upon substitution of V_{l1} from Eq. (A1), $V(l)^{n'M',n_1'M_1'}_{nM,n_1M_1}$ is given by Eq. (A1) with each $(4\pi/2l+1)^{1/2}\mathcal{Y}_{l\mu}(\hat{r})$ replaced by

$$\langle n',L',S,J',M'\left|\left(\frac{4\pi}{2l+1}\right)^{1/2}\mathcal{Y}_{l\mu}(r)\right|n,L,S,J,M\rangle$$

$$= (-1)^{J'-M'+L'+S+J+l} \begin{pmatrix} J' & l & J \\ -M' & \mu & M \end{pmatrix} (2J+1)^{1/2}(2J'+1)^{1/2}(2L'+1)^{1/2}(2L+1)^{1/2} \begin{Bmatrix} L' & J' & S \\ J & L & l \end{Bmatrix} \begin{pmatrix} L' & l & L \\ 0 & 0 & 0 \end{pmatrix} \mathcal{R}_{n'L',nL}, \tag{A3}$$

where

$$\mathcal{R}_{n'L',nL} = \int_0^\infty R_{n'L'}(r) r^l R_{nL}(r)\, dr,$$

and the appropriate quantum numbers in Eq. (A2) are to be used for atoms A and B. Equation (A3) follows from Eqs. (5.4.1), (7.1.7), and (5.4.5) of Ref. 27.

We will use only the leading Van der Waals term in the energy $V_{\alpha MM_1}(R)$ of Eq. (3b), which corresponds to replacing

$$|\langle A(nM)B(n_1M_1)|\, V'(\vec{R})\, |A(k\mathfrak{M})B(k_1\mathfrak{M}_1)\rangle|$$

with $R^{-3}V(1)^{k\mathfrak{M},k_1\mathfrak{M}_1}_{nM,n_1M_1}$. Thus Eq. (3b) becomes

$$V_{\alpha MM_1}(\vec{R}) = E_n + E_{n_1} - C_{\alpha MM_1}R^{-6},$$

where

$$C_{\alpha MM_1} = \sum_{\substack{kk_1\\ \mathfrak{M}\mathfrak{M}_1}} (E_k + E_{k_1} - E_n - E_{n_1})^{-1} \left| V(1)^{k\mathfrak{M},k_1\mathfrak{M}_1}_{nM,n_1M_1} \right|^2. \quad \text{(A4)}$$

Also taking only the leading term in $V'(R)$ of Eq. (3a) leads to $R^{-2-l}V(l)^{k\mathfrak{M},k_1\mathfrak{M}_1}_{nM,n_1M_1}$ for the matrix element in Eq. (3a), where $l=2$ (or 1) for the case of a change (or no change) in the total parity of the initial α and final α' adiabatic states. The mixed-in atomic product states of course have $L'=L\pm1, L_1'=L_1\pm1$ for the $l=1$ case and $L'=L\pm2$ or 0, $L_1'+L_1\pm1$ for the $l=2$ case. The labeling of atoms A and B has so far been arbitrary. Hereafter, to avoid unnecessary terms we will include mixing by the V_{qd} operator and not V_{dq}. No generality is thereby lost, but the redundancy in the labeling of atoms A or B for the $l=2$ case is removed. Substituting these modified Eqs. (3a) and (3b) into Eq. (4), abbreviating $A(nM)B(n_1M_1)$ as nM,n_1M_1, including the l index in $P(b,v,\omega)$, and dropping the $\frac{1}{2}E_0e^{-i\omega t}$ part of $E_0\cos\omega t$ then yields

$$P(b,v,\omega,l) = \sum_{MM'M_1M_1'} \frac{1}{g_n g_{n_1}} \left| \int_{-\infty}^{\infty} dt \left(\langle nM, n_1M_1| + \sum_{kk_1\mathfrak{M}\mathfrak{M}_1} \frac{V(l)^{k\mathfrak{M},k_1\mathfrak{M}_1}_{nM,n_1M_1}\langle k\mathfrak{M}, k_1\mathfrak{M}_1|}{(E_n+E_{n_1}-E_k-E_{k_1})R^{2+l}} \right) \right.$$
$$\times \exp\left(i\int_{-\infty}^{t} \frac{C_{\alpha MM_1}}{\hbar R^6(t')}\, dt' \right) \left(\frac{\vec{E}_0\cdot e\vec{r}}{2\hbar} e^{i(\omega-\omega_0)t} \right) \exp\left(-i\int_{-\infty}^{t} \frac{C_{\alpha' MM_1'}}{\hbar R^6(t')}\, dt' \right)$$
$$\left. \times \left(|n'M'n_1'M_1'\rangle + \sum_{k'k_1'\mathfrak{M}'\mathfrak{M}_1'} \frac{V(l)^{n'M',n_1'M_1'}_{k\mathfrak{M},k_1\mathfrak{M}_1}|k'\mathfrak{M}', k_1'\mathfrak{M}_1'\rangle}{E_{n'}+E_{n_1'}-E_{k'}-E_{k_1'})R^{2+l}} \right) \right|^2. \quad \text{(A5)}$$

Since $\vec{r}=\Sigma\vec{r}_i$ is a single electron operator, the radiative perturbation only connects product states which have the same quantum numbers for one of the atoms. Specifically, either $k\mathfrak{M}=n'M'$ or $k_1\mathfrak{M}_1=n_1'M_1'$, and $nM=k'\mathfrak{M}'$ or $n_1M_1=k_1'\mathfrak{M}_1'$ is required in Eq. (A5). The above choice of only the V_{qd} operator requires that for the $l=2$ case we identify atom B as off-diagonal with respect to $V_r(t)$. This convention can be taken for $l=1$ as well; then only terms $k\mathfrak{M}=n'M'$ and $k'\mathfrak{M}'=nM$ contribute to Eq. (A5), which reduces to

$$P(b,v,\omega,l) = \sum \frac{e^2/\hbar^2}{4g_ng_{n_1}} \left| \int_{-\infty}^{\infty} \frac{dt}{R(t)^{l+2}} \exp i\left[(\omega-\omega_0)t - \int_{-\infty}^{t} dt' \frac{C_{\alpha MM_1}-C_{\alpha' M'M_1'}}{\hbar R^6(t')} \right] \right.$$
$$\left. \times \left(\sum V(l)^{n'M',k_1\mathfrak{M}_1}_{nM,n_1M_1} \frac{\langle k_1\mathfrak{M}_1|\vec{E}_0\cdot\vec{r}|n_1'M_1'\rangle}{E_n+E_{n_1}-E_{n'}-E_{k_1}} + \sum V(l)^{n'M',n_1'M_1'}_{nM,k_1'\mathfrak{M}_1'} \frac{\langle n_1M_1|\vec{E}_0\cdot\vec{r}|k_1'\mathfrak{M}_1'\rangle}{E_{n'}+E_{n_1'}-E_n-E_{k_1'}} \right) \right|^2. \quad \text{(A6)}$$

Note that the expression in large parentheses is the pair of consecutive collisional and radiative perturbations which induce the transition, as indicated diagrammatically in Eqs. (1b′) and (2a′).

We will now consider the effect of the molecular axis rotation. For $\vec{E}_0$ directed along $\hat{z}$, the laboratory z axis, $\vec{E}_0\cdot\vec{r}=E_0r(\frac{4}{3}\pi)^{1/2}Y_{10}(\theta,\phi)$, where θ and ϕ are laboratory frame angles. We perform two successive Euler angle rotations, first through angles α,β,γ to a primed collision frame with $\vec{b}$ along $\hat{x}'$ and $\vec{v}$ along $\hat{z}'$, then through angles $\alpha',\beta',\gamma'=0,\theta(t),0$ to a double-primed frame with $\hat{z}''$ along $\vec{R}(t)$ (see Fig. 3). Due to the transformation properties[27] of the Y_{lm}, we then have

$$\langle nLSJM|\vec{E}_0\cdot\vec{r}|n'L'S'J'M'\rangle = E_0\sum_{m,m'} \mathfrak{D}^1_{0m'}(\alpha,\beta,\gamma)\mathfrak{D}^1_{m'm}[0,\theta(t),0]\langle nLSJM|r_m|n'L'S'J'M'\rangle. \quad \text{(A7)}$$

Here $r_m\equiv r(\frac{4}{3}\pi)^{1/2}Y_{lm}(\theta'',\phi'')$ is in the $\hat{Z}''=\hat{R}$ frame in which the atomic basis states are quantized, so that Eq. (A3) applies in Eq. (A7) with $r_m=(\frac{4}{3}\pi)^{1/2}\mathcal{Y}_{lm}(r)$.

Taking the angular average of Eq. (A7) in Eq. (A6) yields

$$P(b,v,\omega,l)_{\rm av}=\int_0^{2\pi}\frac{d\alpha}{2\pi}\int_0^{\pi}\frac{-\sin\beta d\beta}{2}\int_0^{2\pi}\frac{d\gamma}{2\pi}P(b,v,\omega,l)$$

$$=\sum_{\substack{MM'M_1M_1'\\ m=1,0,-1}}\frac{e^2E_0^2}{4\hbar^2 g_n g_{n_1}}\left|\sum_{k_1k_1'}F(nMn_1M_1,n'M'n_1'M_1',k_1k_1',ml)\right|^2$$

$$\times\sum_{q=1,0,-1}a_{qm}\left|Z(\omega-\omega_0,l,C_{\alpha MM_1}-C_{\alpha'M'M_1'},U_q)\right|^2, \tag{A8}$$

where

$$Z(\omega-\omega_0,l,C,U_q)\equiv\int_{-\infty}^{\infty}\frac{dt}{R(t)^{l+2}}U_q\exp i\left((\omega-\omega_0)t-\int_{-\infty}^{t}dt'\frac{C}{\hbar R^6(t')}\right),$$

$$a_{qm}=\tfrac{1}{6}[(2+q-q^2)(1-m^2)+m^2],\quad U_{-1}=1,\quad U_0=\sin\theta(t),\quad U_1=\cos\theta(t),$$

and

$$F(nMn_1M_1,n'M'n_1'M_1',k_1k_1',ml)\equiv V(l)^{n'M',k_1\mathfrak{M}_1}_{nM,n_1M_1}\frac{\langle k_1\mathfrak{M}_1|r_m|n_1'M_1'\rangle}{E_n+E_{n_1}-E_{n'}-E_{k_1}}+V(l)^{n'M',n_1'M_1'}_{nM,k_1'\mathfrak{M}_1'}\frac{\langle n_1M_1|r_m|k_1'\mathfrak{M}_1'\rangle}{E_{n'}+E_{n_1'}-E_n-E_{k_1'}},$$

with $\mathfrak{M}_1=M+M_1-M'$ and $\mathfrak{M}_1'=M'+M_1'-M$. Here a_{qm} times $U_q(t)U_q(t')$ is the angular average of

$$\sum_{m'}\mathfrak{D}^1_{0m'}(\alpha,\beta,\gamma)\mathfrak{D}^1_{m'm}[0,\theta(t),0]\sum_{m''}\mathfrak{D}^1_{0m''}(\alpha,\beta,\gamma)\mathfrak{D}^1_{m''m}[0,\theta(t'),0],$$

where terms of $m'\neq m''$ angular average to zero. Also the same m occurs after angular average in the remaining two $\mathfrak{D}^1(\cdots)$ and in both terms of $F(\cdots)$, since $\mathfrak{M}_1-M_1=M_1'-\mathfrak{M}_1'$ is required in Eq. (A5), from the diagonal property of $V(l)$ with respect to total M. If the $U_q[\theta(t)]$ are removed from the time integral $\sum_q\int d\theta\, a_{qm}U_q^2=\frac{1}{3}$ is obtained, corresponding to the averaged projection of $\hat{E}_0$ along the molecular axis. The $V(l)$ are given by Eqs. (A1)–(A3). Note also that only $m=(M_1-M_1')+(M-M')$ contribute with $m=0,\pm1$.

Equation (A8) with the C_α and $V(l)$ given by Eqs. (A1)–(A4) is the general result. The $F(\cdots)$ part of Eq. (A8) determines the amplitude of each $MM_1M'M_1'$ contribution to $P(b,v,\omega,l)_{\rm av}$, while the spectral shape is fixed by the remaining time-dependent terms or $Z(\omega-\omega_0,\ldots)$. Six different forms of $Z(\omega-\omega_0,\ldots)$ occur on Eq. (A8), those for $q=-1,0,1$ and for $l=1$ or 2. Thus for the $\Delta V(R)\propto R^{-6}$ case under consideration the b and v averages [Eq. (5)] of only these six $Z(\omega-\omega_0,\ldots)$ are sufficient to describe the line shape for all $\Delta L\leq 2$ cases of Eqs. (1) and (2).

We can reduce Z, in which $R(t)=(b^2+v^2t^2)^{1/2}$, to a dimensionless form $Z'(\omega-\omega_0,l,C,U_q)$ $=b^{l+1}vZ(\omega-\omega_0,l,C,U_q)$ in terms of dimensionless variables

$$\delta\equiv(\omega-\omega_0)b/v,\quad x\equiv\cos\theta(t)=vt/(b^2+v^2t^2)^{1/2},$$

$\gamma\equiv C/\hbar b^5v$, where $C\equiv C_{\alpha MM_1}-C_{\alpha'M'M_1'}$ and $\gamma\equiv\gamma^{\alpha'M'M_1'}_{\alpha MM_1}$ is implied, and $U_1=x$, $U_0=(1-x^2)^{1/2}$, $U_{-1}=1$:

$$Z'(\delta,l,\gamma,U_q)=\int_{-1}^{1}dx\,(1-x^2)^{(l-1)/2}U_q\exp\left[i\left(\frac{-x\delta}{(1-x^2)^{1/2}}+\gamma\int_{-1}^{x}dy\,(1-y^2)^{3/2}\right)\right]. \tag{A9}$$

Equations (A8) and (5b) in (5a) yield

$$\frac{T(\omega,l)}{[A(n)][B(n_1)]}=\frac{2\sqrt{\pi}e^2E_0^2}{v_0(C/\hbar v_0)^{2l/5}\hbar^2g_ng_{n_1}}\sum_{\substack{mq\\ MM'M_1M_1'}}\left|\sum_{k_1k_1'}F(nMn_1M_1n'M'n_1'M_1',k_1,k_1',ml)\right|^2a_{qm}L(\omega-\omega_0,C,l,U_q), \tag{A10}$$

where

$$L(D,l,U_q)\equiv L(\omega-\omega_0,C,l,U_q)=\int_0^{\infty}\frac{dB}{B^{2l+1}}\int_0^{\infty}dV\,Ve^{-V^2}\left|Z'\left(\delta=\frac{DB}{V},l,\gamma=B^{-5}V^{-1},U_q\right)\right|^2$$

is a dimensionless line shape with order of magnitude 1 at $\omega=\omega_0$ or $D=0$. We have defined dimensionless variables

$$V=v/v_0,\quad D=(\omega-\omega_0)(C/\hbar v_0)^{1/5}v_0,\quad\text{and}\quad B=b(C/\hbar v_0)^{-1/5},$$

where $v_0=(2kT/\mu)^{1/2}$ is the natural unit of velocity and $(C/\hbar v_0)^{1/5}$ of length for collisions with C_6R^{-6} inter-

actions. A set of $\alpha MM_1, \alpha' M' M_1'$ indices are implicit on B, C, and D. Substitution of Eq. (A10) into Eqs. (6) and (7) then yields k_ν and $Q(\omega, I)$.

Equation (A10) can be simplified considerably by using the approximation of an $MM'M_1M_1'$ averaged $\overline{C}$ in L and taking $\sum_q a_{qm} L(\omega-\omega_0, C, l, U_q) \cong \frac{1}{3} L(\omega-\omega_0, \overline{C}, l, U_q=1)$. Then with k_1, L_1'', J_1'', M_1'' quantum numbers implied by k_1 (the intermediate state of atom B) and noting that the k_1' refers to the same set of states as k_1, Eq. (A10) becomes

$$\frac{T(\omega,l)}{[A(n)][B(n_1)]} \cong \frac{2\sqrt{\pi}e^2E_0^2}{3v_0(\overline{C}/\hbar v_0)^{2I/5}\hbar^2 g_n g_{n_1}} L(\omega-\omega_0, \overline{C}, l, 1)\mathfrak{F}(nn_1, n'n_1') , \tag{A11}$$

where

$$\begin{aligned}\mathfrak{F}(nn_1, n'n_1') \equiv & \sum_{\substack{mMM'M_1M_1' \\ L_1'J_1'M_1'}} \left| \sum_{k_1} F(nMn_1M_1, n'M'n_1'M_1', k_1L_1''J_1''M_1'', ml) \right|^2 \\ = & (l+1)(2J+1)(2J'+1)(2L+1)(2L'+1) \begin{Bmatrix} L & J & S \\ J' & L' & l \end{Bmatrix}^2 \begin{pmatrix} L & l & L' \\ 0 & 0 & 0 \end{pmatrix}^2 \mathfrak{R}^2_{nL,n'L'} \\ & \times \Bigg[\sum_{J_1'' L_1''} \frac{(2J_1''+1)(2J_1+1)(2L_1''+1)^2(2L_1+1)(2J_1'+1)(2L_1'+1)}{3} \\ & \times \begin{Bmatrix} L_1 & J_1 & S_1 \\ J_1'' & L_1'' & 1 \end{Bmatrix}^2 \begin{Bmatrix} L_1' & J_1' & S_1 \\ J_1'' & L_1'' & 1 \end{Bmatrix}^2 \begin{pmatrix} L_1 & 1 & L_1'' \\ 0 & 0 & 0 \end{pmatrix}^2 \begin{pmatrix} L_1' & 1 & L_1'' \\ 0 & 0 & 0 \end{pmatrix}^2 \Bigg] \\ & \times \Bigg[\sum_{k_1} \left(\frac{e^2}{(E_n - E_{n'}) + (E_{k_1} - E_{n_1})} + \frac{e^2}{-(E_n - E_{n'}) + (E_{k_1} - E_{n_1})} \right) \mathfrak{R}_{n_1 L_1, k_1 L_1''} \mathfrak{R}_{k_1 L_1'', n_1' L_1''} \Bigg]^2 . \end{aligned}$$

The terms in the first large square brackets reduce to

$$\frac{2J_1'+1}{3} \begin{pmatrix} L' & 1 & 1 \\ 0 & 0 & 0 \end{pmatrix}^2$$

for the common case of $L_1 = 0$, as occurs in the examples.

Class 1: *ns-n'D* transitions

We now consider a $nS \rightarrow n'D$ transition of atom A, where B is a noble gas or other $L_1 = 0$ atom as in the examples of Eqs. (1a) and (1b). The particular components of the adiabatic states responsible for the (1b) transition are given in Sec. II A. For an atom A of spin S and B a noble gas k_ν is, from Eqs. (6) and (A10) with $l = 2$,

$$\frac{k_\nu}{[A(n)][B(n_1)]} = \frac{16\pi^{3/2}\omega(e^2/\hbar c)}{v_0(C/\hbar v_0)^{4/5}(2S+1)} \sum_{\substack{MM' \\ mq}} \left| \sum_{k_1 k_1'} F(nMn_1 0, n'M'n_1 0, k_1 k_1', m2) \right|^2 a_{qm} L(\omega-\omega_0, C_{\alpha M0} - C_{\alpha' M'0}, 2, U_q) , \tag{A12}$$

where $C_{\alpha M0}$ for the S state is independent of M and $C_{\alpha' M'0}$ for the D state is a function of $|M'|$. From Eqs. (A1)–(A3) and (A8),

$$F(nMn_1 0, n'M'n_1 0, k_1 k_1', m2) = \frac{e^2}{5^{1/2}} \left(\frac{2J'+1}{1+2m^2} \right)^{1/2} \begin{pmatrix} S & 2 & J' \\ -M & m & M' \end{pmatrix} \mathfrak{R}_{nS,n'D} \left| \mathfrak{R}_{n_1 S, k_1 P} \right|^2 f(E) , \tag{A13}$$

where

$$-f(E) = \frac{1}{(E_{k_1} - E_{n_1}) - (E_n - E_{n'})} + \frac{1}{(E_{k_1} - E_{n_1}) + (E_n - E_{n'})} \cong \frac{2}{E_{k_1} - E_{n_1}} ,$$

$$2 \sum_{k_1} \frac{|\mathfrak{R}_{n_1 S, k_1 P}|^2}{E_{k_1} - E_{n_1}} = \frac{3\alpha_B}{e^2} ,$$

and α_B is the noble gas polarizability.[18] This approximation is in error by $(E_n - E_{n'})^2/(E_{k_1} - E_{n_1})^2$, which is small when $E_{k_1} - E_{n_1}$ refers to a noble-gas perturber. As an example, for $S = 0$ as for group-II atoms or Eq. (1a), Eq. (A13) yields

$$\sum_{k_1 k_1'} |F(n0n_1 0, n'M'n, 0, k_1 k_1', m2)|^2 = \Delta(m - M') \frac{9\alpha_B^2 |\mathcal{R}_{nS,n'D}|^2}{5(1+2m^2)}, \tag{A14}$$

where $\Delta(m - M')$ is 0 for $m - M' \neq 0$ and only $m = 0, \pm 1$ occurs.

From Eqs. (A1)–(A4), the energy approximation in Eq. (A13) and the expression for α_B below Eq. (A13) we obtain the C_6 coefficients of an $nLJM$ state against a noble gas

$$C_{\alpha M0} = e^2 \langle r_{nL}^2 \rangle \alpha_B h(J, L, M), \tag{A15}$$

where

$$h(L, J, M) = \sum_{\substack{\text{all } L'J'M' \\ \mu = 0, \pm 1}} 2 \begin{pmatrix} J' & 1 & J \\ -M' & \mu & M \end{pmatrix}^2 \frac{(2J+1)(2J'+1)(2L+1)(2L'+1)}{1+3\mu^2} \begin{Bmatrix} L' & J' & S \\ J & L & 1 \end{Bmatrix}^2 \begin{pmatrix} L' & 1 & L \\ 0 & 0 & 0 \end{pmatrix}^2$$

and $\langle r_{nL}^2 \rangle = \int R_{nL}^2 r^2 dr$. This energy approximation is appropriate for predominately single-electron states,[24] including most excited states. For an S state on atom A, $h(0, J, M) = 1$, while for $L > 0$ the M average of $h(L, J, M)$ is also 1, i.e.,

$$\langle h(L, J, M) \rangle \equiv (2J+1)^{-1} \sum_M h(L, J, M) = 1 \quad \text{and} \quad \overline{C}_{nL} = e^2 \langle r_{nL}^2 \rangle \alpha_B . \tag{A16}$$

For the case of an nS-$n'D$ transition against a noble gas the approximate Eq. (A11) in (6) reduces to

$$\frac{k_\nu}{[A][B]} \cong \frac{16\pi^{3/2}\omega(e^2/\hbar c)}{v_0(\overline{C}/\hbar v_0)^{4/5}} \mathcal{R}_{nS,n'D}^2 \alpha_B^2 g(J') L(\omega - \omega_0, \overline{C}, l = 2, U_q = 1), \tag{A17}$$

where $g(J') = (2J'+1)/5(2S+1)$ is the fractional strength of the J' component of the D-state multiplet and α_B is the noble gas polarizability.

Type (2) or "Radiative collisions"

We choose the Ca + Sr example of a "radiative collision" since this has been observed. Here atom B, the Ca, undergoes an electric quadrupole transition and atom A, the Sr, an electric dipole, as in Eq. (2′) with $\Delta = 1, \Delta_1 = 2$. The components of the molecular adiabatic states responsible for the transition are indicated in Sec. IIA. The quasistatic wing intensity is given by Eq. (10) with $P = 3$ and $D_{\alpha M M_1'}^{\alpha' M' M_1'}$ given below Eq. (A10). The line core is given by Eq. (A10), where n refers to $\mathrm{Sr}(5\,^1P_1)$, n_1 to $\mathrm{Ca}(4\,^1S_0)$, n' to $\mathrm{Sr}(5\,^1S_0)$, n_1' to $\mathrm{Ca}(6\,^1S_0$ or $5\,^1D_2)$, and k_1 and k_1' to $\mathrm{Ca}(k_1\,^1P_1)$ or $\mathrm{Ca}(k_1'\,^1P_1)$:

$$\frac{T(\omega)}{[\mathrm{Sr}(5\,^1P_1)][\mathrm{Ca}(4\,^1S_0)]} = \frac{2\sqrt{\pi}\, e^2 E_0^2 \mathcal{R}_{5S,5P}^2}{v_0(C/\hbar v_0)^{2/5}\hbar^2 3} \times \left[\sum_{k_1} \left(\frac{e^2}{(E_{k_1 P} - E_{4S}) - (E_{5P} - E_{5S})} + \frac{e^2}{(E_{k_1 P} - E_{n_1' L_1'}) + (E_{5P} - E_{5S})} \right) \mathcal{R}_{4S,k_1 P} \mathcal{R}_{k_1 P, n_1' L_1'} \right]^2$$

$$\times \left[\sum_{M M_1' m q} \frac{4(2L_1'+1)}{3(1+3M^2)} \begin{pmatrix} 1 & 1 & L_1' \\ -M & m & M_1' \end{pmatrix}^2 \begin{pmatrix} 1 & 1 & L_1' \\ 0 & 0 & 0 \end{pmatrix}^2 a_{qm} L(\omega - \omega_0, C_{\alpha M0} - C_{\alpha' 0 M_1'}, 1, U_q) \right]. \tag{A18}$$

For comparison, the approximation in Eq. (A11) reduces to Eq. (A18) with the expression in the second square brackets of (A18) replaced by

$$\frac{2(2L_1'+1)}{9} \begin{pmatrix} L_1' & 1 & 1 \\ 0 & 0 & 0 \end{pmatrix}^2 L(\omega - \omega_0, \overline{C}, 1, 1). \tag{A19}$$

---

[1] M. Lapp, Phys. Lett. 23, 553 (1966); and references therein.

[2] J. A. Gwinn, P. M. Thomas, and J. F. Kielkopf, J. Chem. Phys. 48, 568 (1968); F. Besombes, J. Granier, and R. Granier, Opt. Commun. 1, 161 (1969); A. Tam, G. Moe, W. Park, and W. Happer, Phys. Rev. Lett. 35, 85 (1975); W. Happer, G. Moe, and A. Tam, Phys. Lett. 54A, 405 (1975); J. G. Eden, B.E. Charrington, and J. T. Verdeyen, IEEE J. Quantum Electron. QE-12, 698 (1976).

[3] H. T. Powell, J. R. Murray, and C. K. Rhodes, Appl. Phys. Lett. 25, 730 (1974).

[4] P. Julienne, M. Krauss, and W. Stevens, Chem. Phys. Lett. 38, 374 (1976), and references therein.

[5]G. Moe, A. C. Tam, and W. Happer, Phys. Rev. A 14, 349 (1976).
[6]K. Niemax, J. Quant. Spectrosc. Radiat. Transfer 17, 125 (1977).
[7]L. Gudzenko and S. I. Yakavlenko, Zh. Eksp. Teor. Fiz. 62, 1686 (1972) [Sov. Phys.-JETP 35, 877 (1972)]; V. S. Lisitsa and S. I. Yakavlenko, *ibid.* 66, 1550 (1974) [*ibid.* 39, 759 (1974)].
[8]S. E. Harris and D. B. Lidow, Phys. Rev. Lett. 33, 674 (1974) [34, 172(E) (1975)]; and S. E. Harris, D. B. Lidow, R. W. Falcone, and J. F. Young, in *Tunable Lasers and Applications*, edited by A. Mooradian, T. Jaeger, and P. Stokseth (Springer-Verlag, New York, 1976).
[9]D. B. Lidow, R. W. Falcone, J. F. Young, and S. E. Harris, Phys. Rev. Lett. 36, 462 (1976) [37, 1590(E) (1976)]; and R. W. Falcone, W. R. Green, J. C. White, J. F. Young, and S. E. Harris, Phys. Rev. A 15, 1333 (1977).
[10]S. Geltman, J. Phys. B 9, L569 (1976).
[11]J. I. Gersten and M. H. Mittleman, J. Phys. B 9, 383 (1976).
[12]S. Y. Chen and M. Takeo, Rev. Mod. Phys. 29, 20 (1957).
[13]A. J. Barnard, J. Cooper, and E. W. Smith, J. Quant. Spectrosc. Radiat. Transfer 14, 1025 (1974).
[14]A. Giusti-Suzar and E. Roueff, J. Phys. B 8, 8 (1975); 8, 852 (1975).
[15]D. N. Stacey and J. Cooper, J. Quant. Spectrosc. Radiat. Transfer 11, 1271 (1971).
[16]R. E. Hedges, D. Drummond, and A. Gallagher, Phys. Rev. A 6, 1519 (1972).
[17]J. Cooper, "Comments on the Theory of Satellite Bands," JILA Report No. 111 (1973), Joint Institute for Laboratory Astrophysics, University of Colorado, Boulder, Colo. 80309 (unpublished).
[18]A. Dalgarno and W. D. Davidson, Adv. Atom. Mol. Phys. 2, 1 (1966).
[19]T. Holstein, Phys. Rev. 79, 744 (1950).
[20]G. K. Oertel and L. P. Shomo, Astr. J. Suppl. 16, 175 (1968).
[21]E. E. Nikitin, in *The Excited State in Chemical Physics*, edited by J. Wm. McGowan (Wiley-Interscience, New York, 1975), Chapter V.
[22]J. Pascale and J. Vandeplanque, J. Chem. Phys. 60, 2278 (1974).
[23]J. Kielkopf, Phys. Rev. A 5, 484 (1972).
[24]P. Julienne (private communication).
[25]H. Friedrich and E. Trefftz, J. Quant. Spectrosc. Radiat. Transfer 9, 333 (1969).
[26]W. L. Wiese, M. W. Smith, and B. M. Miles, *Atomic Transition Probabilities, Sodium through Calcium*, Natl. Bur. Stds. Spec. Publ. No. NSRDS-NBS 22 (U.S. GPO, Printing Office, Washington, D.C., 19xx).
[27]A. R. Edmonds, *Angular Momentum in Quantum Mechanics* (Princeton U.P., Princeton, N.J., 1960).